AGU PUBLICATIONS

Space Weather

REVIEW ARTICLE
10.1002/2016SW001450

Special Section:
Reprise of "Space Weather" 2001 Monograph

Variability and predictability of the space environment as related to lower atmosphere forcing

H.-L. Liu[1]

[1] High Altitude Observatory, National Center for Atmospheric Research, Boulder, Colorado, USA

Key Points:
- Review the role of waves from lower atmosphere in thermosphere/ionosphere (TI) variability
- Elucidate how predictability of the TI is affected by the lower atmosphere
- Highlight outstanding questions in studying lower/upper atmosphere coupling

Correspondence to:
H.-L. Liu,
liuh@ucar.edu

Citation:
Liu, H.-L. (2016), Variability and predictability of the space environment as related to lower atmosphere forcing, *Space Weather*, *14*, 634–658, doi:10.1002/2016SW001450.

Received 17 JUN 2016
Accepted 29 AUG 2016
Accepted article online 8 SEP 2016
Published online 24 SEP 2016

Abstract The Earth's thermosphere and ionosphere (TI) are characterized by perpetual variability as integral parts of the atmosphere system, with intermittent disturbances from solar and geomagnetic forcing. This review examines how the TI variability is affected by processes originating from the lower atmosphere and implications for quantifying and forecasting the TI. This aspect of the TI variability has been increasingly appreciated in recent years from both observational and numerical studies, especially during the last extended solar minimum. This review focuses on the role of atmospheric waves, including tides, planetary waves, gravity waves, and acoustic waves, which become increasingly significant as they propagate from their source region to the upper atmosphere. Recent studies have led to better understanding of how these waves directly or indirectly affect TI wind, temperature, and compositional structures; the circulation pattern; neutral and ion species transport; and ionospheric wind dynamo. The variability of these waves on daily to interannual scales has been found to significantly impact the TI variability. Several outstanding questions and challenges have been highlighted: (i) large, seemingly stochastic, day-to-day variability of tides in the TI; (ii) control of model error in the TI region by the lower atmosphere; and (iii) the increasing importance of processes with shorter spatial and temporal scales at higher altitudes. Addressing these challenges requires model capabilities to assimilate observations of both lower and upper atmosphere and higher model resolution to capture complex interactions among processes over a broad range of scales and extended altitudes.

1. Introduction

The compositional and thermal structures of the Earth's thermosphere and ionosphere (TI) are of central importance for space weather and space climate research, because they interact with the solar radiative and particulate inputs, determine the atmosphere drag on space vehicles and debris, and affect radio communication and GPS signals. The TI is a highly variable system displaying a broad range of temporal and spatial scales, and to understand, quantify, and forecast these variabilities are major objectives of space environment studies. The TI composition and energetics are primarily determined by solar radiation and can be strongly disturbed by radiative, magnetic, and particulate changes due to solar flares, coronal mass ejection (CME), geomagnetic solar storms, or magnetospheric substorms. The onsets of these events are determined by the solar and/or magnetospheric states, and their predictability thus depends on the predictability of the Sun, the solar wind, and the magnetosphere, though the TI responses to such large disturbances also depend on the state of the TI. These large events are intermittent, but the TI still displays persistent variabilities in their absence. These variabilities can have significant magnitude and can be disruptive to radio communication and GPS signals (e.g., ionospheric irregularities in *E* or *F* regions). Knowledge of the variabilities also enables better quantification of the prestorm conditions and leads to better prediction of storm time responses.

These variabilites of the TI during "quiet time" periods have been thought to be generally caused by perturbations originating from the lower atmosphere. For example, statistical studies of the critical frequency of the ionospheric F_2 peak (f_oF_2) data from over 100 stations by *Forbes et al.* [2000] found that under geomagnetic quiet conditions ($Kp < 1$) the F_2 region peak plasma density variability (N_mF_2), measured via standard deviation, ranges from 25 to 35% of the mean for high-frequency (hours to 2days) and 15 to 20% of the mean for low-frequency (2–30days) components. With the very low level of geomagnetic forcing and minimal impact of $F_{10.7}$ variability on the *F* region, these variabilities are thought to be from "meteorological forcing." *Rishbeth and Mendillo* [2001] reached a similar conclusion, that the meteorological forcing is responsible for ~15% of the N_mF_2 standard deviation, by analyzing the total N_mF_2 standard deviation, the standard

deviation of the *Ap* index, and sensitivity of the F_2 region peak plasma density to *Ap* index. Pathways by which the lower atmosphere affects the upper atmosphere, however, were not well understood at that time. Thanks to both new observations, in particular those during the last extended solar minimum, and the use of numerical models that treat the whole atmosphere as an integrated system (see *Akmaev* [2011] for a review of whole atmosphere modeling), there has been rapid progress in our understanding. In this paper, we will review the recent development in our understanding of TI variability, and the implications for the predictability, as related to lower atmosphere forcing, especially through atmospheric waves. This review complements the review of this subject by *Laštovička* [2006], by focusing more on progresses in numerical modeling studies, especially the ones within the last decade. The paper is organized as follows: Section 2 reviews the tidal and planetary-scale wave variability on long and short time scales, including the seemingly stochastic day-to-day tidal variability and how they affect the TI; section 3 discusses factors that impact predictability of the upper atmosphere and the need for whole atmosphere data assimilation; section 4 discusses the significant role that mesoscale processes, in particular gravity waves, play in the TI and the challenge and recent progress in quantifying gravity waves. A brief summary is presented in section 5.

2. Upper Atmosphere Variability as Related to Tides and Other Planetary-Scale Waves

Atmospheric waves of various scales play a key role in coupling the lower and upper atmosphere, because they can cause large atmospheric perturbations and can transport momentum, energy, and atmosphere constituents. Waves are generated when the essential atmosphere balance states, such as hydrostatic and geostrophic balances, are perturbed. Common examples include gravity waves, tides, Kelvin waves, and Rossby waves; see, e.g., *Andrews et al.* [1987] and *Forbes* [1995] for detailed discussions of these atmospheric waves. A brief summary of essential features of these waves are given in Table 1. A note on nomenclature is as follows: Rossby waves are also often referred to as planetary waves, while planetary-scale waves generally refer to tides, Rossby waves, and equatorial waves, especially the latter two in this review. When referring to tides, the following convention is adapted: tidal period in terms of harmonics of a day (D for diurnal, S for semidiurnal, T for terdiurnal, etc.), propagation direction (E for eastward propagating, W for westward propagating), and zonal wave number. For example, DW1 is for diurnal westward propagating tide with zonal wave number 1. A majority of wave sources are found in the troposphere, such as deep convection, frontal system, orography, diabatic heating/cooling, land-sea contrast, and instabilities. In addition, diabatic heating from absorption of solar ultraviolet (UV) radiation by stratospheric ozone is a source of atmospheric thermal tides. Adjustment processes associated with the winter stratospheric jet can excite gravity waves. Nonlinear interactions between primary waves can also generate secondary waves. The waves can propagate into the middle and upper atmosphere under favorable wind and temperature conditions and modulate the winds, thermal and compositional structures, and electrodynamics. The wave sources and the propagation condition (background wind and temperature) can vary significantly over space and time, and as a result waves in the upper atmosphere display large variability and contribute to the variability of the space environment. Since predictability reflects the strength of a signal as compared to the variability, in particular stochastic variability of a system, processes with well-defined periodicity, such as atmospheric waves, can thus enhance predictability, while variability of wave amplitudes and periods (and thus phases), on the other hand, may negatively affect predictability.

2.1. Atmospheric Tides and Their Long-Term Variability

Atmospheric tides, including thermal and lunar gravitational tides with migrating and nonmigrating components, have been known to play an important role in the upper atmosphere and upper atmosphere variability [e.g., *Forbes*, 1995] and in ion-neutral coupling. Observations have shown that tidal signals can extend into the upper thermosphere, including the ionospheric dynamo region [e.g., *Häusler et al.*, 2007; *Häusler and Lühr*, 2009; *Forbes et al.*, 2008, 2009; *Oberheide et al.*, 2009; *Häusler et al.*, 2010], in spite of the strong molecular damping of the waves in the thermosphere. This likely results from the exponential density decrease and fast thermal conduction. Tides can cause temperature and density modulations and are responsible for the formation of midnight temperature maximum (MTM) and midnight density modulation (MDM) [*Miyoshi et al.*, 2009; *Akmaev et al.*, 2010; *Lei et al.*, 2011; *Ruan et al.*, 2014]. Tidal modulation of ion-neutral coupling is exemplified by the observational and modeling studies of the four wave structures in the equatorial ionosphere anomaly (EIA) and equatorial electrojet (EEJ) [*Sagawa et al.*, 2005; *Immel et al.*, 2006; *Hagan et al.*, 2007; *Lühr et al.*, 2008],

Table 1. A Brief Summary of the Major Atmospheric Waves of Interest to the Thermosphere and Ionosphere

	Primary Restoring Force	Wave Sources	Temporal/Spatial Scales	Propagation
Solar thermal tides	Buoyancy	Solar radiative heating, latent heat	Harmonics of a solar day/planetary	Migrating: westward following the Sun Nonmigrating: not following the Sun
Lunar tides	Buoyancy	Lunar gravitational force	Harmonics of a lunar day/planetary	Following the Moon
Rossby waves, mixed Rossby-gravity waves	Coriolis force/buoyancy	Tropospheric processes: topography, land-ocean contrast, diabatic heating	Days to quasi-stationary/planetary	Westward relative to background wind
Equatorial waves: Kelvin waves, equatorial Rossby waves, equatorial mixed Rossby-gravity waves, equatorial inertio-gravity waves	Buoyancy/Coriolis force	Tropical tropospheric processes: deep convection	Days/planetary	Equatorially trapped Kelvin waves: eastward Equatorial Rossby mixed Rossby-gravity waves: westward Equatorial inertio-gravity waves: eastward and westward
Gravity waves	Buoyancy	Deep convection, orography, frontal system, adjustment of jet, body forcing from wave breaking	Longer than buoyancy period and less than inertial period/km to thousands of kilometers	Horizontal and vertical
Acoustic waves	Air pressure	Deep convection, orography	Shorter than buoyancy period/km to hundreds of kilometers	Horizontal and vertical

and ionospheric responses during stratospheric sudden warming (SSW) [*Goncharenko et al.*, 2010; *Yue et al.*, 2010; *Chau et al.*, 2012]. Tidal winds affect ion-neutral coupling through the ionosphere *E* and *F* region wind dynamo [*Richmond et al.*, 1976; *Forbes and Lindzen*, 1976; *Richmond and Roble*, 1987; *Millward et al.*, 2001; *Liu et al.*, 2010a; *Liu and Richmond*, 2013], as well as by modulating plasma transport and ion-neutral collisions in the *F* region [*Wan et al.*, 2012; *Lei et al.*, 2014]. Tides with large amplitudes at middle to high latitudes (such as migrating and nonmigrating semidiurnal components), as well as those at lower latitudes, can contribute to the modulation of ionospheric electrodynamics [e.g., *Liu and Richmond*, 2013]. The relative importance of the *E* and *F* region wind dynamo can be affected by the solar activity, which determines the damping and penetration height of tidal waves [*Oberheide et al.*, 2009; *Liu et al.*, 2010b], as well as the Pederson and Hall conductivities [*Liu and Richmond*, 2013].

Upper atmosphere tides display large variability over long and short time scales [e.g., *Forbes et al.*, 2008] and can thus contribute to the variability of the space environment on climate and weather scales. Tidal variability is caused by changes in wave forcing, propagation conditions (including resonance conditions), and interaction among tides and with other waves (e.g., other tides, planetary waves, and gravity waves). Over interannual time scales, tides in the mesosphere/lower thermosphere (MLT) region are modulated by El Niño and the Southern Oscillation (ENSO), as evidenced by observations [*Lieberman et al.*, 2007; *Warner and Oberheide*, 2014] and by numerical simulations [*Pedatella and Liu*, 2012, 2013]. The numerical simulations determined that the ENSO-induced MLT variability is 10–30% and the ionospheric variability is 10–15%. ENSO-related changes in tropospheric diabatic heating is the primary cause of variability of diurnal migrating tide (DW1) and some of the nonmigrating diurnal tidal components (e.g., eastward wave 2 and 3, DE2 and 3). The DE2 and 3 are also affected by the background atmospheric changes during ENSO, while some other nonmigrating

components are affected by nonlinear interaction with planetary waves (which changes during ENSO as found by *Sassi et al.* [2004] and *Manzini et al.* [2006]).

On interannual time scales, tides in the MLT region are also modulated by the quasi-biennial oscillation (QBO) [*Burrage et al.*, 1996; *Wu et al.*, 2008a, 2008b; *Xu et al.*, 2009]. During the easterly/westerly phase (QBO-E/W), DW1 and DE3 are weaker/stronger and the migrating semidiurnal tide (SW2) is stronger/weaker. This dependence has been reproduced in whole atmosphere model simulations [e.g., *Liu*, 2014]. Since the propagation and resonance amplification of tides are found to be sensitively dependent on the zonal mean wind [*Forbes and Vincent*, 1989; *Forbes and Zhang*, 2012], it has been proposed that the QBO modulation could be caused by changes in vertical wavelength and dissipation and changes in ozone heating; however, numerical experiments using the Global Scale Wave Model (GSWM) suggested that neither could explain the QBO modulation of the diurnal migrating tide (DW1) [*Hagan et al.*, 1999]. Some tidal components are also well known to display an annual and semiannual variation. For example, DW1 in the MLT reaches a primary maximum around March equinox and a secondary maximum around September equinox, and SW2 amplitude peaks in the winter hemisphere [*Burrage et al.*, 1995; *Wu et al.*, 2011]. *McLandress* [2002] demonstrated that DW1 is dependent on the latitudinal shear of the zonal mean zonal wind (thus, the zonal mean vorticity) in the summer mesosphere. The vorticity change alters the tidal propagation through modifying the equivalent depth of the tides.

2.2. Short-Term Tidal Variability and Tidal Interaction With Other Planetary-Scale Waves

Short-term variability (including variability with scales of day to day to a month) is of interest in space weather studies. Perturbations originating from the lower atmosphere can play an important role in the short-term variability of the upper atmosphere. For example, continuous lidar measurements by *She et al.* [2004] showed that the diurnal temperature amplitude in the MLT region can double or even triple from one day to the next [*Liu et al.*, 2007]. According to the comparative modeling study by *Liu et al.* [2007], this rapid change could result from interaction between tides and planetary waves. Such interaction can excite diurnal nonmigrating components and modulate modes of migrating components and thus lead to changes of the total diurnal signal.

Quasi-stationary planetary waves (QSPWs) are the strongest planetary wave events in the winter stratosphere and mesosphere, and they can alter the stratospheric and mesospheric circulation pattern during stratospheric sudden warming (SSW) events [*Scherhag*, 1952; *Matsuno*, 1971]. Due to wave-mean flow interactions, the QSPWs undergo rapid increases and decreases during life cycles of SSWs (with time scales of weeks). Tides, including both thermal tides and lunar tides, have been shown to display large variability during SSWs as manifested in both the neutral atmosphere and ionosphere [e.g., *Goncharenko et al.*, 2010; *Fejer et al.*, 2010, 2011; *Park et al.*, 2012; *Yamazaki et al.*, 2012; *Yamazaki*, 2013; *Wu and Nozawa*, 2015; *Chau et al.*, 2015], and possible mechanisms considered include nonlinearly interaction with the QSPWs, as well as changes in zonal mean zonal winds and tidal sources [e.g., *Liu and Roble*, 2002; *Pancheva et al.*, 2009; *Chang et al.*, 2009; *Sridharan et al.*, 2012; *Liu et al.*, 2010a; *Fuller-Rowell et al.*, 2010; *Forbes and Zhang*, 2012]. Due to their large magnitude change in a short time duration, QSPW and SSW events provide exemplary cases to gain insights into the link of the lower and upper atmosphere through complex interactions among tides, planetary waves, and mean circulation. QSPW forcing on the mean wind may not always lead to a reversal of the stratospheric jet or even a minor SSW, but they can still contribute to MLT variability. One such example is the variability around the equinox transition period, when QSPWs start to become strong. Their interaction with the mean flow can lead to short-term changes of wind and temperature in the middle and upper atmosphere, termed "hiccup" by *Matthias et al.* [2015], with structures similar to SSW but smaller magnitudes.

In addition to QSPWs, traveling planetary waves (TPWs) and equatorial waves (EWs) and their interactions with tides and mean flow can also cause MLT variability. Well-known examples of TPWs and EWs of interest to the MLT include waves with periods of 5–7days (also referred to as 6.5days) [*Hirota and Hirooka*, 1984; *Wu et al.*, 1994; *Talaat et al.*, 2001, 2002; *Lieberman et al.*, 2003; *Sridharan et al.*, 2008] and quasi-2days [*Muller and Nelson*, 1978; *Rodgers and Prata*, 1981; *Harris and Vincent*, 1993; *Wu et al.*, 1993; *Garcia et al.*, 2005; *Pancheva et al.*, 2006; *Hecht et al.*, 2010] and ultrafast Kelvin waves (UFKW, Kelvin waves with periods of 3–4days) [*Salby et al.*, 1984; *Lieberman and Riggin*, 1997; *Gasperini et al.*, 2015]. Episodes of strong 5–7day wave and quasi-2day wave (QTDW) are observed in the MLT around equinox (5–7day wave) and around January-February and July-August (QTDW) [*Talaat et al.*, 2001; *Wu et al.*, 1993]. These window periods are determined by the wave propagation (wave guide) and amplification (baroclinic/barotropic instability) conditions, which

in turn are dependent on the background winds [*Plumb*, 1983; *Meyer and Forbes*, 1997; *Salby and Callaghan*, 2001; *Liu et al.*, 2004; *Yue et al.*, 2012a]. In particular, the occurrence of QTDW with specific wave number (wave number 2, 3, or 4) may depend sensitively on the background wind conditions [*Gu et al.*, 2016]. UFKWs, on the other hand, do not seem to have a clear seasonal dependence. TPWs may also become large around the time of SSW due to favorable propagation and amplification conditions [*McCormack et al.*, 2009; *Chandran et al.*, 2013; *Sassi et al.*, 2013]. When these planetary waves become large, they can cause tidal variability either through nonlinear wave-wave interaction or through altering the background winds [*Palo et al.*, 1999; *Pancheva*, 2006; *Chang et al.*, 2011; *Forbes and Moudden*, 2012; *Pedatella et al.*, 2012; *Sassi and Liu*, 2014; *Moudden and Forbes*, 2014].

2.3. Tidal Variability on Day-To-Day Scales

Knowledge of the tidal and planetary-scale wave interaction can enhance predictability of the upper atmosphere, since the planetary-scale waves up to the stratopause are generally well quantified and predicted. For example, the forecast experiment by *Wang et al.* [2014] demonstrated that the SSW event in 2009 could be captured 1–2weeks prior to the peak warming. Furthermore, since QSPWs and TPWs display clear seasonal dependence, tidal variability from tidal-planetary wave interaction would be seasonally dependent, too. A recent modeling study [*Liu*, 2014] suggests, however, that there is also an irregular or "stochastic" aspect of the day-to-day tidal variability. As shown in *Liu* [2014], amplitudes of migrating and nonmigrating tides in the upper atmosphere from the Whole Atmosphere Community Climate Model with thermosphere and ionosphere extension (WACCM-X) simulations vary significantly from one day to the next. The day-to-day time scale is shorter than the time scales associated with planetary wave variability (weeks to a month), and it appears to be ubiquitous and does not show any clear seasonal, annual, or interannual dependence (while planetary waves usually do). The exact causes of the tidal day-to-day variability in the MLT have not been systematically studied, but there are several plausible ones: (1) It is known from previous studies that the atmosphere is a deterministic chaotic system that displays perpetual stochastic vacillations [*Lorenz*, 1969] and that the middle/upper atmosphere is no exception [*Liu et al.*, 2009]. It is conceivable that the tidal day-to-day variability is a manifestation of the stochastic whole atmosphere system. (2) Tidal propagation is sensitively dependent on the winds as discussed earlier. Therefore, the tidal variability in the MLT is affected by the variability of global winds along the tidal propagation path from the source region to the MLT. (3) The tidal wave sources, which are often tied to processes in the troposphere weather system, are likely to be variable.

Since predictability is closely tied to the time scales of variabilities, there is a need to better quantify the latter for zonal mean zonal wind and tides in light of the second and third points. One way of measuring the time scales is to compute the correlation time of a quantity by integrating the autocorrelation function. Figure 1 shows the correlation time of the zonal mean zonal wind, as well as the amplitudes of three main tidal components (DW1, SW2, and DE3), calculated using detrended time series of these quantities from a 20-model year simulation of WACCM-X (detailed discussion can be found in *Liu* [2014]). The correlation time of zonal mean zonal wind is long in the stratosphere (weeks to months) and shorter in the troposphere, mesosphere, and thermosphere (less than 5days at most places). In the stratosphere, the main dynamical driving is by planetary waves, which vary on time scales of weeks or longer, and they are thus responsible for the longer correlation times. Dynamical processes with shorter time scales, on the other hand, becomes predominant in the mesosphere and lower thermosphere, and as a result these regions are more variable. In the upper thermosphere, the short correlation time of zonal mean zonal wind is a result of strong dissipative damping. The correlation time is determined by signal strength and signal variability. It is thus expected that the correlation time should follow the wave amplitude, yet should be reduced by the wave variability. It is seen from Figures 1b–1d that the tidal correlation time in general follows the structure of the respective tidal amplitude in the latitudinal direction but not necessarily in the vertical direction. For example, DW1 amplitude peaks in the lower thermosphere, but its correlation time is the longest in the stratosphere (~18days) and becomes shorter in the MLT (~3days). For DW1, the decrease of correlation time with altitude is consistent with that of the zonal mean zonal wind, which is an indication of the impact of the wind modulation. The correlation times of SW2 and DE3 are more complex, though they are still comparable with or shorter than the correlation time of zonal mean zonal wind in the MLT (maximums of 8days for SW2 and 4days for DE3). The wind modulation thus may still play an important role in the variability of these tides. The stochastic feature and the short correlation time of the diurnal tidal amplitude from the model is consistent with the autocorrelation analysis of observed diurnal tidal amplitudes by *Phillips and Briggs* [1991], though it is noted that the observations were made at one location (Buckland Park, 35°S, 138°E) and thus include all diurnal components.

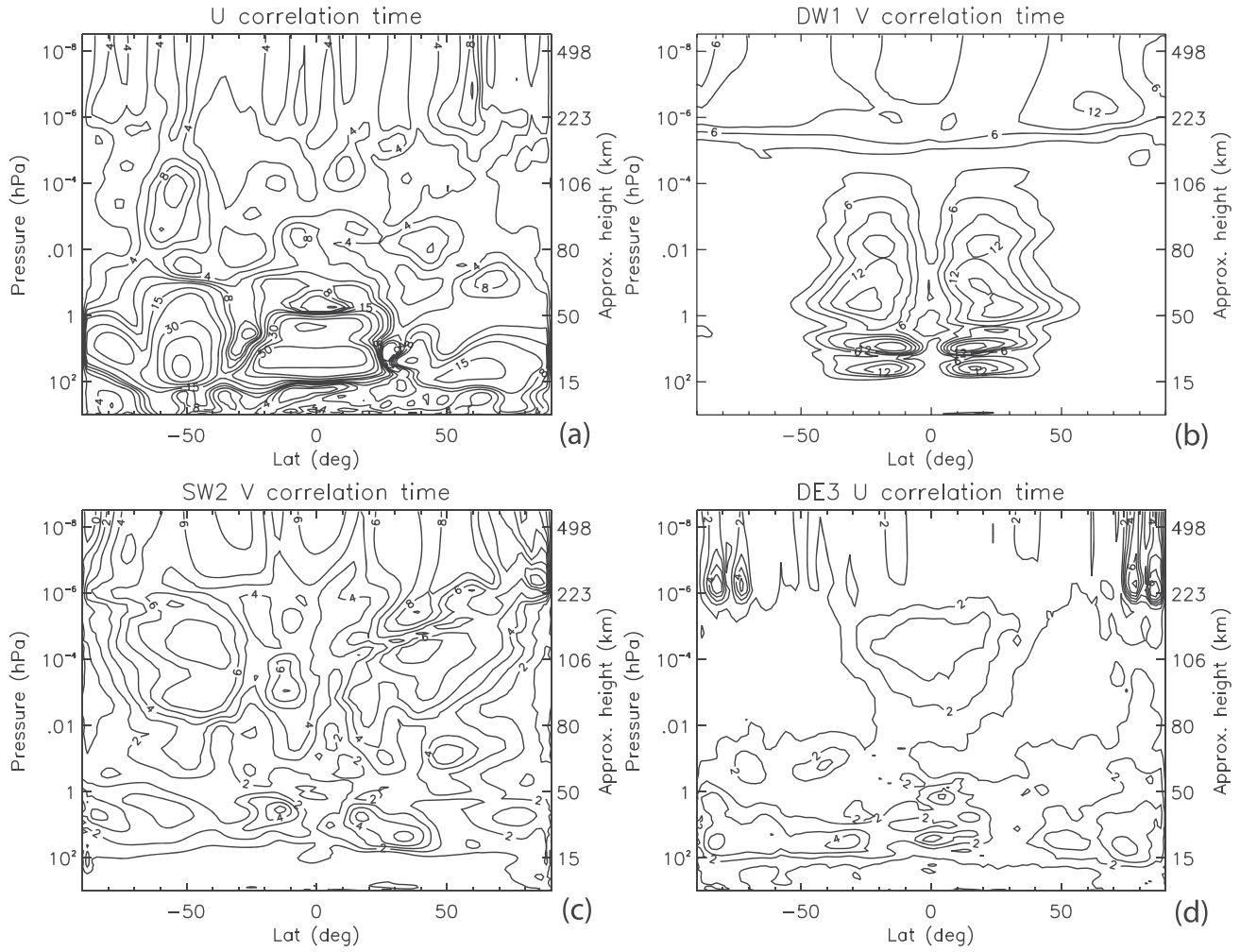

Figure 1. Correlation time (unit: day) of (a) zonal mean zonal wind and amplitudes of (b) migrating diurnal tide (DW1), (c) migrating semidiurnal tide (SW2), and (d) nonmigrating diurnal tide DE3. Contour intervals: Figure 1a: 2days for correlation time up to 10days and then 15, 20, 30, 40, and 50days; Figure 1b: 3days; Figures 1c and 1d: 1day.

The spatial correlation of tidal amplitudes is shown in Figure 2. To elucidate the differences in short and long-term variability, the detrended time series are decomposed into low-frequency components, obtained by smoothing the time series with a boxcar average over 10days, and high frequency components (referred to as day-to-day variable components). Figures 2a–2c are the correlation patterns for the high-frequency components, and Figures 2d–2f are for the low-frequency ones. The correlation coefficients for the day-to-day variable tides decay rapidly, dropping to 0 over a distance of ~20 km in altitude and 20–30° in latitude. Lagged correlation for the day-to-day variable tides has also been examined. With a lag of 2days, the correlation coefficients for DW1 are small (0.15) but still significant down to ~70 km, while the correlation coefficients for SW2 and DE3 are less than 0.1 below 80 km. No significant correlation is found beyond 2days for the day-to-day variability of these tides below 80 km. In contrast, significant correlation is found for long-term tidal variability down to the troposphere (DW1), stratosphere (SW2), and stratopause DE3). The correlation analysis thus suggests that the day-to-day tidal variability in the MLT is indeed more stochastic. It is not directly related to the variability of tidal sources in the troposphere and/or the stratosphere. Long-term tidal variability, on the other hand, is more closely related to tidal source variability.

Apart from interaction with a complex global wind system, including various large-scale waves, a potential source of tidal variability is that caused by tidal interaction with gravity waves [*Walterscheid*, 1981]. Previous studies using either mesoscale models or global scale models have demonstrated the interaction of these

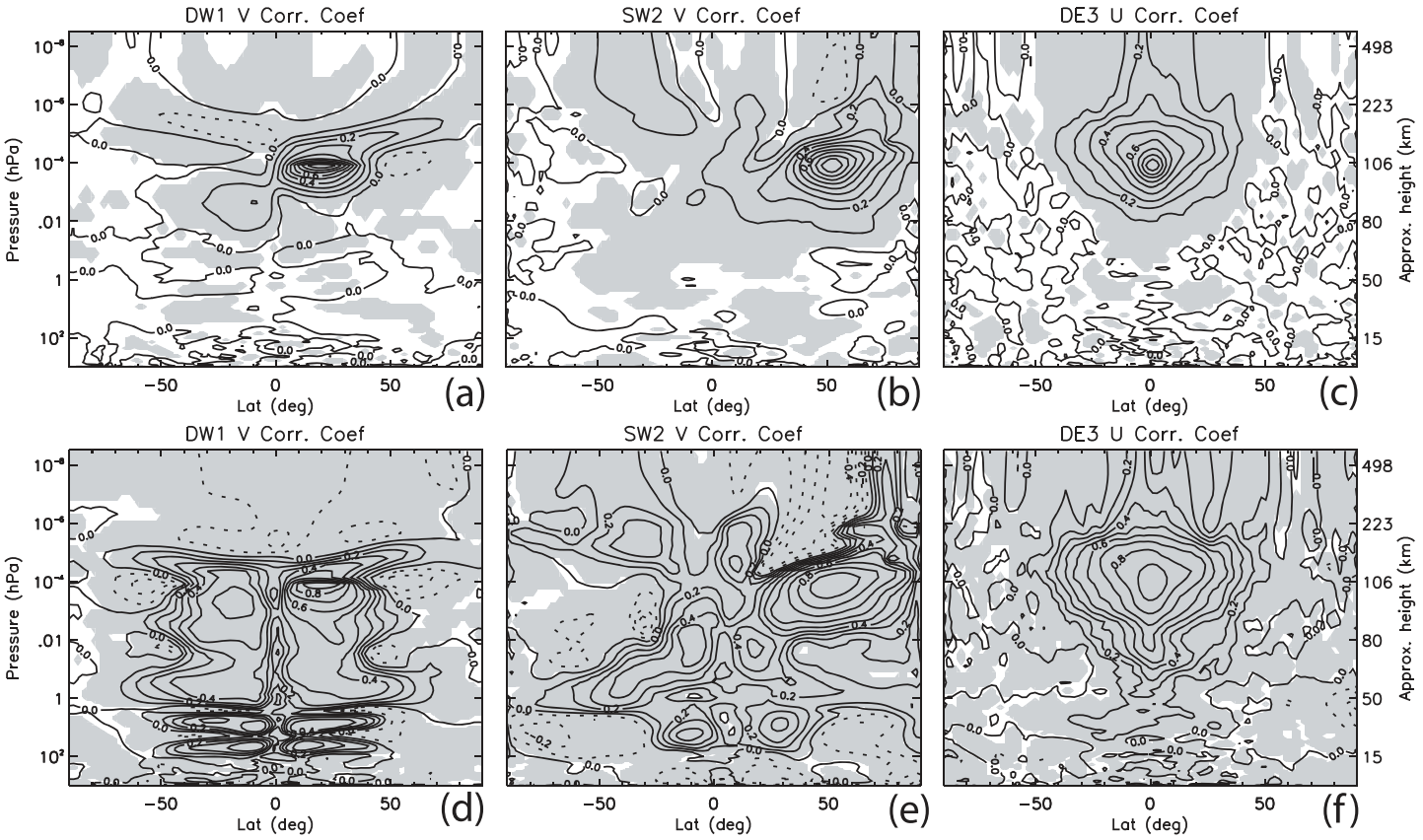

Figure 2. Spatial correlation coefficients of tidal amplitudes with (top row) short-term and (bottom row) long-term variability. (a and d) Migrating diurnal tide (DW1), (b and e) migrating semidiurnal tide (SW2), and (c and f) nonmigrating diurnal tide (DE3). The reference points are at the latitudes where the respective tidal amplitudes maximize in the MLT region. Statistically significant correlation is highlighted with gray shade. Contour intervals: 0.1.

two types of waves [*Liu and Hagan*, 1998; *Liu et al.*, 2000; *Ortland and Alexander*, 2006; *Liu et al.*, 2014b]. Gravity wave instability and wave breaking, which are modulated by tidal temperature and winds, can lead to momentum deposition and heat flux change and can in turn modify the tidal amplitude and phase. Since the gravity waves are known to be highly variable spatially and temporally, their interaction with tides can be an important source of tidal variability. The variability due to gravity wave-tidal interactions, however, is still poorly quantified. The challenge for self-consistently studying such interaction stems from the large-scale difference between these two types of waves, which will be discussed later.

2.4. Ionospheric Variability Caused by Tides and Other Planetary-Scale Waves

There are several known ways in which atmospheric waves contribute to ionospheric variability. These include wave modulation of *E* and/or *F* region wind dynamo, ion-neutral coupling and field-aligned transport in the *F* region, and transport of neutral species in the mesosphere and lower thermosphere (which in turn affects neutral and plasma densities higher up).

Tidal waves can propagate deep into the middle and upper thermosphere with their large propagating speed and modulate the ionospheric structures. A numerical study by *Millward et al.* [2001] determined that the ionosphere prereversal enhancement (PRE) depends sensitively on the amplitude and phase of the semidiurnal tide. The variability of the tides can thus contribute to the variability of the ionosphere, as evidenced by observational and numerical studies of the ionosphere during SSW. As discussed earlier, tides undergo large variability during SSW, likely resulting from a combination of tidal-planetary wave and tidal-gravity wave interactions, changes of tidal propagation and resonance conditions, and changes of wave sources. Since tides can penetrate into the upper thermosphere, tidal wind changes lead to changes of the *E* and *F* region dynamo. Therefore, even though the QSPWs responsible for SSWs cannot usually impact the ionospheric *E* or *F* region, they can have indirect impact by modulating tidal variability [*Liu et al.*, 2010a]. A thorough review of ionospheric variability during SSW is given by *Chau et al.* [2012].

In addition to affecting the wind dynamo, tides can also affect the ionospheric plasma density through ion-neutral coupling. *Wan et al.* [2012] and *Lei et al.* [2014] found that nonmigrating tides directly perturb the thermospheric neutral density. Through ion-neutral coupling, the thermospheric perturbations contribute to ionospheric variability, though these modeling studies found that this contribution is minor compared with the variability due to the wind dynamo.

Numerical studies by *Müller-Wodarg and Aylward* [1998], *Yamazaki and Richmond* [2013], and *Jones et al.* [2014] have found that tides can affect the transport in the mesosphere and lower thermosphere, mainly by changing the meridional and vertical circulation, and thus affect the thermospheric and ionosphere compositions. As shown by a recent numerical study by *Pedatella et al.* [2016], the MLT circulation change caused by short-term tidal change during SSW can be comparable or even dominant over the circulation changes caused by gravity wave forcing [*Miyoshi et al.*, 2015]. The net effect is to decrease atomic oxygen and increase molecular oxygen and nitrogen, similar to enhanced eddy diffusion. The change extends to the upper thermosphere by the effective molecular diffusion. Although these numerical studies have focused on migrating diurnal and semidiurnal tides, the same mechanism is likely to be applicable to other migrating and also nonmigrating components with significant amplitudes in the MLT. On the other hand, tidal modulation of atomic oxygen recombination rate [*Akmaev and Shved*, 1980; *Forbes et al.*, 1993] is found to be insignificant in the MLT region, probably due to the very long chemical lifetime of atomic oxygen therein [*Yamazaki and Richmond*, 2013].

TPWs can also cause ionospheric variability. *Chen* [1992] identified 2day oscillations in the equatorial ionization anomaly and proposed that it is caused by QTDW modulation of dynamo and field-aligned transport. Oscillations of *F* region electron density with periods 2 and 6.5days are identified from midlatitude ground-based observations and are assumed to be caused by TPWs [*Altadill and Apostolov*, 2001]. Analyses of concurrent neutral dynamics and ionospheric observations provided further evidence linking planetary-scale waves with ionospheric variability: *Pancheva et al.* [2006] related QTDW observed in MLT neutral wind measurements to quasi-2day oscillations of both *F* region electron density and ionospheric current; *Gu et al.* [2014] found clear correspondence between 6day wave from temperature and wind measurements by Sounding of the Atmosphere using Broadband Emission Radiometry (SABER) and TIMED Doppler Interferometer (TIDI) on NASA's Thermosphere Ionosphere Mesosphere Energetics Dynamics (TIMED) satellites with 6day oscillation in total electron content (TEC). Ionospheric variabilities have also been related to TPWs (and also UFKWs) with periods between 5 and 6days identified in MLT neutral winds and in National Centers for Environmental Prediction (NCEP) reanalysis data [*Pancheva et al.*, 2008]. As noted by *Pancheva et al.* [2006], the ionospheric oscillations sometimes do not match neutral atmosphere TPWs exactly in the timing of the peak amplitudes or zonal wave number. For such events, it is possible that TPWs indirectly impact ionospheric variability, especially the *F* region, by modulating variability of tides, which can penetrate to higher altitudes.

Numerical studies have further elucidated the mechanisms how TPWs affect ionospheric wind dynamo. Numerical studies by *Yue et al.* [2012a, 2012b] found that although QTDWs can reach large amplitudes near the summer mesopause due to baroclinic/barotropic instability, they tend to decrease rapidly with altitude and thus do not significantly perturb *E* region dynamo. On the other hand, QTDWs can gain large amplitude in the equatorial lower thermosphere/*E* region as they propagate upward through the wave guide. This branch of the QTDWs, as shown in *Yue et al.* [2012b], perturbs the ionospheric electric potential, $E \times B$ drift, and electron density. The numerical simulation, however, found no evident tidal modulation by QTDW. Furthermore, since QTDWs originate from the winter lower atmosphere, they are likely to nonlinearly interact with the QSPWs. One of the child waves from the QTDW wave number 3 (W3) and QSPW wave number 1 interaction is QTDW wave number 2 (W2), and it has been found to become large in the MLT region and ionosphere [*Pancheva et al.*, 2006; *Tunbridge et al.*, 2011]. Numerical experiments by *Gu et al.* [2015] demonstrated that W2 penetrates to higher altitudes (probably due to its larger phase speed) and that W2 and W3 can have comparable contributions to the ionospheric $E \times B$ drift. UFKWs are also shown to propagate to high altitudes: a numerical study by *Chang et al.* [2010] found that a strong UFKW can be quite strong in the *F* region. The study determined that the UFKW affects ionosphere variability mainly through the ionospheric wind dynamo. This is consistent with the observation that UFKWs can affect the development of spread *F* by modulating the vertical drift [*Abdu et al.*, 2015].

Like tidal waves, TPWs may affect thermospheric and ionospheric variability by species transport between the mesosphere and thermosphere. A numerical study by *Yue and Wang* [2014] found that the dissipation of QTDW in the MLT region leads to circulation change, which in turn enhances the vertical down-gradient

transport and mixing near the turbopause. As a result, thermosphere O/N_2 and F_2 peak electron density decreases. Observational evidences of TPW effects on the transport have been provided from analysis of concurrent TIDI, Global Ultraviolet Imager (GUVI), and TEC measurements for multiple episodes of QTDW events [*Chang et al.*, 2014] and 6.5 day wave events [*Gan et al.*, 2015]. Both studies found that the column integrated O/N_2 and TEC decrease during strong TPW events. The percentage TEC changes from both studies range between 15 and 25%, while the column integrated O/N_2 changes are different (~6% in the case of QTDW and 16–24% in the case 6.5 day wave). These are in general agreement with model results by *Yue and Wang* [2014]. And they are also similar in magnitude to the changes caused by tidal waves [e.g., *Yamazaki and Richmond*, 2013]. Recent numerical studies using WACCM-X by *Sassi et al.* [2016] found that during periods of strong TPWs events (with periods between 3 and 10days), the dissipation of TPWs in the lower thermosphere reinforces the mean meridional circulation with stronger upwelling in the tropics and downwelling at high latitudes. This, along with fast molecular diffusion, reduces the O/N_2 and neutral density at high latitudes while slightly increasing these quantities at low latitudes. It should be noted that electrodynamics are not considered in this simulation.

TPWs in the winter hemisphere can propagate equatorward and break at subtropical surf zone in the lower thermosphere, as shown by *Sassi et al.* [2016]. In addition to causing mean flow acceleration, the wave breaking also results in a meridional, down-gradient mixing of constituents. Although this horizontal diffusion is largest below 110 km, the effects on the compositional structure are shown to be significant throughout the thermosphere due to the strong molecular diffusion.

As discussed earlier, there is a stochastic aspect of tidal day-to-day variability, which is ubiquitous and independent of season. Its implication for the ionospheric day-to-day variability was explored by *Liu et al.* [2013]. Hourly wind and temperature outputs from WACCM-X, which displays large day-to-day tidal variability as shown in *Liu* [2014], were used to constrain (often referred to as nudging) the Thermosphere-Ionosphere-Mesosphere-Electrodynamics general circulation model (TIME-GCM) up to ~95 km. As a result of this nudging, migrating and nonmigrating tides in TIME-GCM also show large day-to-day variability with the standard deviation at 25% to 50% of the wave amplitudes. With solar forcing held at a constant minimum condition and geomagnetic forcing at a constant quiet condition, the model produces remarkable day-to-day variability in vertical and zonal $E \times B$ drifts and F_2 peak electron density (N_mF_2). The standard deviations of the drifts and N_mF_2 from the model show clear local time and longitudinal dependence that are consistent with observations. The magnitudes of the standard deviation are 50% or more of those obtained from observations, consistent with the finding by *Rishbeth and Mendillo* [2001] that the meteorological driving may contribute comparably with geomagnetic forcing to the IT day-to-day variability. A numerical study by *Fang et al.* [2013] reached a similar conclusion with regard to tidal forcing and ionospheric longitudinal and day-to-day variability.

The simulated stochastic day-to-day ionospheric variability is reminiscent of the stochastic variability of the ionospheric current system observed by *Briggs* [1984]: the variations of the ionospheric current system seem to be random and are almost uncorrelated from one day to the next. Because the ionospheric wind dynamo and current system are determined by global winds in the thermosphere (weighted by electric conductivities), the lack of global coherence in tidal day-to-day variability, as shown in Figures 2a–2c, implies that the ionospheric day-to-day variability would be stochastic and would not correlate well with tidal variability at a single location. This is consistent with the observational finding by *Phillips and Briggs* [1991], that there is a lack of correlation between the variability of the ionospheric currents and the variability of tidal winds measured at Buckland Park, 35°S, 138°E. *Yamazaki et al.* [2014] demonstrated that the observed day to day of the EEJ can indeed be reproduced from TIME-GCM simulations when the model is constrained by realistic meteorological forcing up to 95 km.

Tidal waves thus play a key role in the thermosphere and ionosphere system, by directly perturbing winds, temperature, electrodynamics, and composition. Their day-to-day variability is thus important in studying the weather of the thermosphere/ionosphere system. Possible causes of the tidal day-to-day variability include dependence of wave propagation on background wind and temperature along the wave path, interactions with planetary waves and gravity waves, and variability of wave sources. In particular, the short autocorrelation time of background wind (Figure 1) and rapid decrease of spatial correlation of day-to-day tidal variability (Figures 2a–2c) demonstrate the challenge of deterministic calculation of tidal day-to-day variability from their sources and the need for constraining the whole atmosphere background.

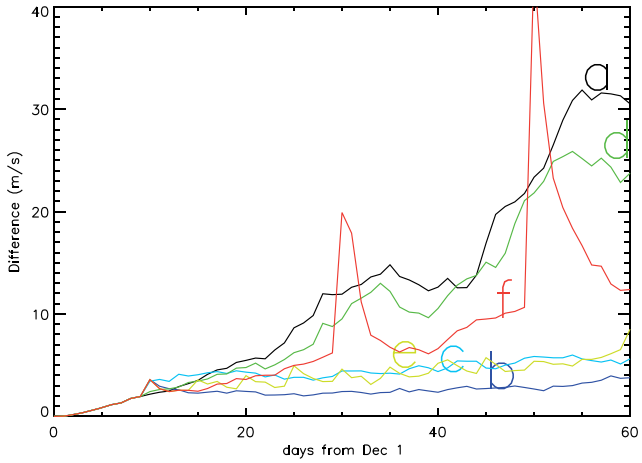

Figure 3. Line a: RMS error in zonal wind between two identical twin WACCM simulations, with case "B" being the base case ("truth") simulation and small perturbations introduced in the initial condition for case "A". Lines b–d: RMS error in zonal wind in "hybrid" simulations with initial conditions from case A above pressure level p_s on 10 December, model reinitialized by results from case B below p_s every 24h, and p_s set to 50hPa, 500hPa, and 700hPa, respectively. Lines e and f: similar to line b but the reinitialization period set to 5days and 20days, respectively. This demonstrates the control of error growth in the middle and upper atmosphere by the lower atmosphere in WACCM [*Liu et al.*, 2009] (©American Meteorological Society. Used with permission).

3. Upper Atmosphere Predictability as Related to Lower Atmosphere Forcing

Climate and weather models are known to display features of deterministic chaos: any initial error will grow exponentially over time, due to complex feedback processes involving nonlinearity and/or instability in the system [e.g., *Lorenz*, 1963, 1969; *Kalnay*, 2003]. The error growth fundamentally limits the forecast capability of the models. It is thus important to study the predictability of the model systems, especially the rate of the error growth and processes determining the error growth, to design and optimize data assimilation schemes to improve forecast skills. Some middle and upper atmosphere models, such as the NCAR Thermosphere-Ionosphere-Mesosphere-Electrodynamics general circulation model (TIME-GCM), show little or no error growth, indicating that nonlinearity does not necessarily lead to chaos. Actually, a recent study by *Shen* [2014] found that nonlinear interaction between modes (as well as parameterized nonlinear eddy dissipation) can improve stability and predictability of a system. On the other hand, stratosphere and stratosphere-mesosphere simulations have shown vacillations between two different flow regimes when the specified tropospheric planetary wave forcing becomes large enough [*Holton and Mass*, 1976; *Yoden*, 1987a, 1987b; *Scaife and James*, 2000]. Using the UK Met Office (UKMO) Stratosphere and Mesosphere Model (SMM), *Gray et al.* [2003] performed ensemble simulations with different levels of tropospheric forcing, and they found that the error growth becomes more pronounced with increasing tropospheric forcing. This suggests that wave-mean flow interaction can be important for the error growth in the stratosphere and mesosphere. The error growth in the whole atmosphere context was examined by *Liu et al.* [2009] using WACCM. By performing identical twin type of experiments, with errors artificially introduced in the initial conditions, they found that the model results start to show clear deviation after 10–20days and that errors become comparable to internal model variability after 40–50days, regardless of the magnitude or scale of the initial error. The time scales are much shorter than those found in the SMM simulations by *Gray et al.* [2003] (50days and 100days, respectively). *Liu et al.* [2009] also found that the error growth is dependent on season and altitude: the largest error growth occurs in the winter stratosphere and both winter and summer MLT, and the smallest error growth in the summer stratosphere. To determine the role of the tropospheric forcing (as compared with wave-mean flow interaction) in error growth, one of the WACCM simulations with imperfect initial condition is repeated, but this time its troposphere is replaced every certain time (Δt) by the base case ("truth") simulation. It is found that if Δt is set to 1day or 5days, shorter than the characteristic error growth time (10–20days), the error in the middle and upper atmosphere in this simulation shows little growth (Figure 3). This study thus demonstrates that the troposphere plays a key role in controlling the error growth of the middle and upper atmosphere models. This has been confirmed later by a WACCM data assimilation experiment using the data assimilation research testbed (DART) ensemble adjustment Kalman filter and synthetic

observations that are generated by sampling a WACCM simulation at the location of real observations [*Pedatella et al.*, 2013]: Using data assimilation to constrain the lower atmosphere reduces the global root mean square error (RMSE) in zonal wind by up to 40% at MLT altitudes. Whole-atmosphere simulations with the lower atmosphere constrained either by data assimilation or nudging to reanalysis results during SSW periods have been able to reproduce tidal and ionospheric variabilities that agree with observations [e.g., *Fuller-Rowell et al.*, 2011; *Jin et al.*, 2012; *Wang et al.*, 2014; *Pedatella et al.*, 2014a].

Several other studies, however, exposed model biases in the mesosphere and thermosphere even when the troposphere and stratosphere are well constrained, mainly due to the incorrect representation of the gravity wave effects. Intercomparisons among four leading whole atmosphere models, GAIA (Ground-to-topside model of Atmosphere and Ionosphere for Aeronomy), HAMMONIA (Hamburg Model of the Neutral and Ionized Atmosphere), WAM (Whole Atmosphere Model), and WACCM-X, by *Pedatella et al.* [2014c] found that although the atmosphere below the stratopause is virtually identical among the four models for a targeted time period (January and February 2009) from data assimilation or nudging, the structure and temporal evolution of mean wind, temperature, and planetary waves in the mesosphere and thermosphere are significantly different in both hemispheres among the model results, as shown in Figure 4. For the zonal mean zonal wind, the height and strength of the wind reversal in the MLT region differ from model to model. GAIA, HAMMONIA, and WACCM-X all produced elevated stratopause following the peak SSW, but the heights, magnitudes, and descending rates of the elevated stratopause are different, while no clear elevated stratopause is seen in WAM simulation. SW2, which has been shown to strongly affect ionospheric variability, is qualitatively similar in these simulations, with a rather strong decrease around peak SSW, followed by a large increase. But the exact timing of the changes, as well as the wave amplitudes, are different in the simulations. Analysis of the model results suggests that differences in effective gravity wave forcing in the MLT are a major cause of the model differences in the mesosphere and thermosphere. This is hardly surprising, since gravity wave forcing is a major driver of MLT dynamics and there exist significant differences and uncertainties in the underlying physics and tuning among different parameterization schemes. Furthermore, *Pedatella et al.* [2014b] found that by only assimilating real observations of the lower atmosphere, WACCM-DART system does not improve the MLT temperature when compared with SABER and Microwave Limb Sounder (MLS) observations. A recent study by *Siskind et al.* [2015] also found that the WACCM simulation with its dynamics constrained up to 92 km by the Navy Operational Global Atmospheric Prediction System-Advanced Level Physics High Altitude (NOGAPS-ALPHA) yields a dramatic improvement in the simulated descent of enhanced nitric oxide and very low methane, over similar WACCM simulation but constrained up to 50 km by Modern-Era Retrospective Analysis for Research and Applications (MERRA). These appear to contradict previous results by *Liu et al.* [2009] and *Pedatella et al.* [2013]. It is noted, however, that in reaching the conclusion that constraining the lower atmosphere helps limiting the error growth in the middle and upper atmosphere, the underlying assumption in "identical twin" experiments by *Liu et al.* [2009] and Observation Simulation System Experiment (OSSE) by *Pedatella et al.* [2014a] is that the model physics is complete. This is certainly not the case: Subgrid processes, such as gravity waves and turbulence, are missing or poorly represented in these whole atmosphere models. On the other hand, it has been found that by better resolving gravity waves, the predictability of the stratosphere and mesosphere is enhanced [*Ngan and Eperon*, 2012]. To improve the representation of the upper atmosphere, therefore, it is necessary to better constrain the model by assimilating upper atmosphere observations, to improve gravity wave parameterization scheme, and/or to directly resolve gravity waves in the model.

4. Importance of Mesoscale Processes for the Upper Atmosphere Variability and Predictability

Gravity waves (GWs) become increasingly important with height, primarily due to the exponential growth of wave amplitudes with the density decrease, as well as their ubiquity in the global atmosphere. Apart from causing large atmosphere perturbations, GWs can deposit wave momentum and interact with large-scale flows when dissipated, due to either instability or molecular damping. As a result, GWs can transfer momentum from their source region to their impact region, making them an important agent for lower and upper atmosphere coupling. GW instability and GW dissipation can also induce turbulent mixing and transport of heat and constituents. A comprehensive review of GWs can be found in *Fritts and Alexander* [2003]. GWs, especially the high-frequency components and secondary GWs from the dissipation of primary waves, can

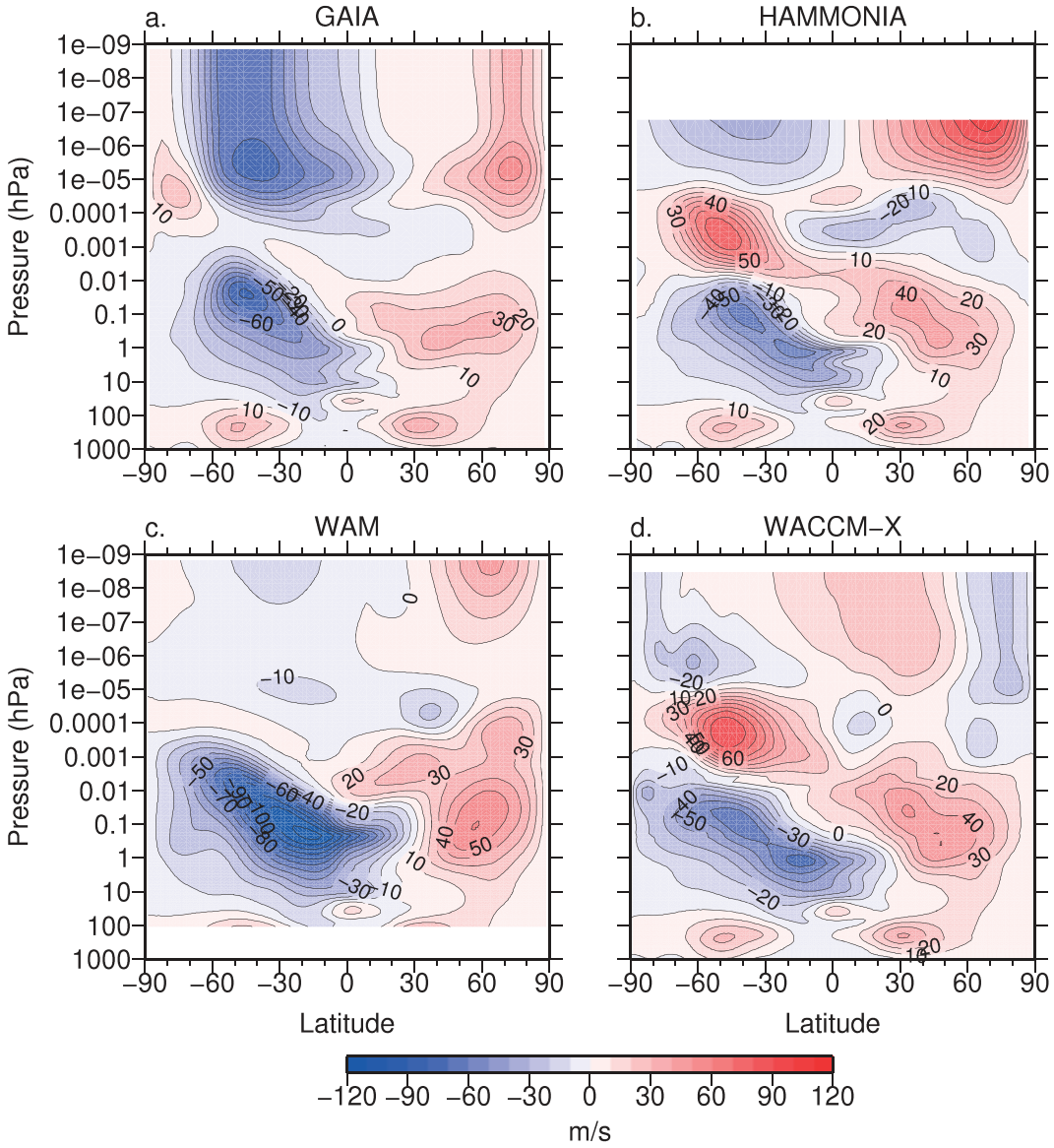

Figure 4. Zonal mean zonal wind averaged from 1 January to 20 February 2009 for (a) GAIA, (b) HAMMONIA, (c) WAM, and (d) WACCM-X. GAIA, HAMMONIA, and WACCM-X are constrained by various reanalysis products up to 12hPa, 1hPa, and 0.002hPa, respectively, while WAM assimilates the standard lower atmosphere observations that influence model results up to 0.1hPa. The background states of the four models thus agree at least up to 12hPa. The zonal winds at higher altitudes, however, are notably different among the four models [*Pedatella et al.*, 2014c] (©American Geophysical Union. Used with permission).

penetrate into the thermosphere and cause thermospheric and ionospheric disturbances [e.g., *Hines*, 1960; *Vadas and Fritts*, 2001; *Vadas*, 2007]. For example, one of the main motivations of the seminal paper by *Hines* [1960] was to explain traveling atmospheric disturbances (TADs) and traveling ionospheric disturbances (TIDs). Observed TIDs have been directly related to wave sources in the lower atmosphere, including deep convection, earthquake, and tsunami [e.g., *Tsugawa et al.*, 2011; *Nishioka et al.*, 2013; *Azeem et al.*, 2015; *Huba et al.*, 2015; *Meng et al.*, 2015]. GWs are thought to drive ionospheric irregularities, such as the midlatitude sporadic *E* layer (Es) (probably along with semidiurnal tides) and equatorial spread *F* (ESF) [e.g., *Kelley et al.*, 1981; *Mathews*, 1998; *Haldoupis*, 2012; *Krall et al.*, 2013b]. They may thus play an important role in ion-neutral coupling and space weather applications. It is noted that wave sources that are capable of generating GWs can also excite acoustic waves at frequencies higher than the buoyancy frequency. Like GWs, the acoustic wave amplitudes increase with altitude and can thus cause large perturbations in the upper atmosphere

[e.g., *Walterscheid et al.*, 2003; *Zettergren and Snively*, 2013]. The acoustic waves can contribute to the thermospheric energetics through viscous heating [e.g., *Hickey et al.*, 2001; *Walterscheid and Hickey*, 2005]. Due to their short temporal scales, direct observation of acoustic waves and assessment of their global impact are challenging. In global models, they are poorly represented due to limited spatial and temporal resolution, as well as the hydrostatic approximation employed by many.

4.1. Challenges to Quantifying Gravity Waves

GWs are a challenging multiscale problem: The wave spatial scales are determined by the many different sources with scales ranging from kilometers to thousands of kilometers and intrinsic wave periods between the buoyancy and inertial periods; the processes they impact range from turbulence to planetary-scale waves and general circulation. They are also highly variable, due to the variability of sources and the sensitive dependence of wave propagation on wind and temperature structures. To account for the broad range of scales and the variability is a stiff challenge for observations and global simulations. Ground-based observations, such as radar, lidar, all-sky imagers, radiosonde, and rockets, have been used to infer GW characteristics, seasonal variation, and vertical profiles of momentum fluxes [e.g., *Fritts and Alexander*, 2003]. Observations at single sites usually provide relatively high cadence and have been used for time/frequency domain analysis. They are generally limited in the spatial coverage and thus in resolving spatial scales of the waves, though they can be expanded by employing observational networks. For example, GW and their source information over North America have been deduced from U.S. radiosonde measurements [e.g., *Wang and Geller*, 2003; *Gong and Geller*, 2010]. Characteristics of gravity waves in the mesosphere, thermosphere, and ionosphere have been determined using a network of all-sky imagers by *Shiokawa et al.* [2000, 2009]. Concentric wave structures in total electron content (TEC) over Japan following the 2011 Tohoku Earthquake have been mapped with high resolution using a dense GPS receiver network by *Tsugawa et al.* [2011]. Using the first no-gap hydroxyl (OH) airglow all-sky imager network (consisting of six imagers), *Xu et al.* [2015] were able to measure multiple and complex GW activity in a contiguous area of 2000 km × 1400 km (east-west/north-south) over China. Extended spatial coverage of GWs has also been provided by airborne measurements, such as the long-duration balloon measurements (VORCORE over Antarctica [*Hertzog et al.*, 2008]) and aircraft measurements (DEEPWAVE over New Zealand and Tasmania [*Fritts et al.*, 2016]). For global coverage of GWs, analyses of satellite observations have provided increasingly comprehensive information on the global distribution and seasonal variation of GWs, including their energy density and absolute momentum flux, from the stratosphere to the lower thermosphere [*Fetzer and Gille*, 1994; *Dewan et al.*, 1998; *Tsuda et al.*, 2000; *Eckermann and Preusse*, 1999; *Ern et al.*, 2004; *Alexander et al.*, 2008; *Wu and Eckermann*, 2008; *Hoffmann and Alexander*, 2009; *Ern et al.*, 2011; *Gong et al.*, 2012; *Sakanoi et al.*, 2011; *Alexander*, 2015; *Miller et al.*, 2015]. Directional GW momentum fluxes in the stratosphere have been deduced recently by *Wright et al.* [2016], by combining the near-coincident Atmospheric Infrared Sounder (AIRS) and MLS measurements and taking advantage of their high horizontal and vertical resolution, respectively. These observations are helping better constrain parameterization schemes used in climate models [*Alexander and Barnet*, 2007; *Alexander et al.*, 2010]. A recent review and intercomparison of various measurements of GWs (and comparisons with parameterized and resolved GWs from general circulation models) was given by *Geller et al.* [2013]. These measurement techniques are sensitive to different temporal and spatial scales, as discussed by *Alexander and Barnet* [2007].

In most general circulation models, GWs are either poorly resolved or not resolved at all, so the wave effects on the large-scale flows need to be parameterized. GW parameterization schemes for the stratosphere and mesosphere are reviewed by *McLandress* [1998], and *Alexander et al.* [2010] reviewed how the parameterization schemes could be better constrained by observations. By accounting for molecular dissipation, a few of the schemes have been extended into the thermosphere [*Garcia et al.*, 2007; *Yiğit et al.*, 2008]. Dissipation of GWs in the thermosphere can lead to excitation of secondary GWs and has been studied by *Vadas* [2007]. With proper tuning, the parameterization schemes have been able to reproduce wind reversals and MLT temperature structures, mesosphere semi-annual oscillation (SAO), and QBO. Recent development of parameterization schemes starts to account for more realistic wave sources as related to deep convection and frontal systems, intermittency, and oblique wave propagation [e.g., *Charron and Manzini*, 2002; *Richter et al.*, 2010; *Kalisch et al.*, 2014], though there remain large uncertainties in specifying wave strength and spectral content. These in turn lead to uncertainties and biases in the models, as discussed in the previous section.

In spite of differences in physical assumptions and uncertainties of parameters involved, all parameterization schemes seek to quantify momentum deposition and eddy diffusion associated with GW dissipation.

These partially address the needs to study coupling across scales and between the lower and upper atmosphere through GWs. The parameterization schemes do not, however, quantify processes that are dependent on GW perturbations, such as ionosphere ion-neutral coupling through ionospheric wind dynamo processes, modulation of polar stratospheric and mesospheric clouds, and temperature-sensitive chemical processes. Numerical simulations by *Vadas and Liu* [2013] and *Liu and Vadas* [2013] demonstrated that secondary GWs could cause large thermosphere and ionosphere perturbations, but the numerical model could only capture secondary waves with horizontal wavelengths larger than ~1000 km. The ability to study ionospheric impact by GWs with smaller scales is fundamentally limited in such model simulations.

4.2. Progress in Mesoscale-Resolving Global Models

In recent years increasing computing power has afforded increasing spatial resolution of general circulation models, including whole atmosphere models. For numerical weather prediction models, it is clearly imperative to resolve down to mesoscales. Current operational models in leading weather centers have reached down to ~10 km and the order of 1 km with nesting in their horizontal resolution. It is shown that tropical precipitation and tropical circulation improve with increasing model resolution [e.g., *Lean et al.*, 2008; *Jung et al.*, 2012]. There have also been exploratory efforts to increase resolution of climate models. The study by *Bacmeister et al.* [2014] using the NCAR CAM with quarter-degree resolution found that the model produces realistic tropical cyclone distributions and interannual variability.

Given the increasing significance of GWs with altitude, global models with extended vertical domain can benefit from increasing resolutions. *Hamilton et al.* [1999] demonstrated that the SKYHI model with higher spatial resolution (35 km horizontally with 160 levels between surface and 85 km) reduced the cold bias during early winter in the southern polar stratosphere and produced a QBO-like oscillation in the equatorial stratospheric zonal mean zonal winds. *Koshyk et al.* [1999] found that the divergence flow (largely associated with resolved GWs) in middle atmosphere models grew more rapidly with altitudes than the rotational flow above the lower stratosphere, and as a result the energy spectra became shallower at higher altitudes. Using an aquaplanet spectral model with triangular truncation at 106 of the spherical harmonic expansion and 63 vertical levels, or T106/L63 (corresponding to ~120 km horizontal resolution at the equator and 600m vertical resolution), *Sato et al.* [1999] resolved stratospheric inertial GWs with characteristics that are similar to observations. They also identified downward wave energy propagation in the winter stratosphere, likely from GW generation from the stratosphere polar night jet. *Watanabe et al.* [2008] developed a middle atmosphere GCM with T213/L256 spatial resolution (~62.5 km at the equator and 300m vertically) and demonstrated that the resolved waves drive a QBO-like oscillation in equatorial stratospheric zonal winds (with a period of ~15 months), and confirmed the vertical change of kinetic energy spectrum toward a shallower structure at high altitudes, as found by *Koshyk et al.* [1999]. The Japanese Atmospheric General circulation model for Upper Atmosphere Research (JAGUAR) is an extension of this middle atmosphere GCM to ~150 km and has been used to study GW forcing on the tides [*Watanabe and Miyahara*, 2009]. By using a whole atmosphere GCM that extends to the upper thermosphere with 1.1° × 1.1° horizontal resolution, *Miyoshi et al.* [2014] showed that the resolved GWs are significant in the thermosphere and that they are modulated by semidiurnal tides (between 100 and 200 km altitude) and diurnal tides (above 200 km). By analyzing results from the ECMWF T799/L91 operational forecast for the 2009 SSW period, *Yamashita et al.* [2010] found significant GW variability in the winter stratosphere associated with changes of the polar night jet and planetary waves during that time period. The GW excitation by the polar night jet is consistent with findings by *Sato et al.* [1999].

Recently, *Liu et al.* [2014a] developed a version of WACCM with horizontal resolution of ~25 km and 209 levels between the Earth surface and ~145 km, enabling the model to effectively resolve waves down to mesoscales (~200 km). GW energy density and its latitude-height structure from the simulations are in general agreement with those obtained from SABER measurements [*Ern et al.*, 2011]. Figure 5 shows zonal mean GW momentum fluxes, averaged over January and July, calculated from this WACCM simulation. They are in general agreement with the momentum fluxes deduced from various satellite measurements [*Geller et al.*, 2013]: a momentum flux maximum is found at middle to high latitudes in the winter hemisphere, especially in the Southern winter hemisphere, and a secondary maximum at subtropical latitudes in the summer hemisphere. The former is likely associated with GWs excited along storm tracks, over orography, and adjustment of stratospheric jet, while the latter is probably from tropospheric deep convection. The latter maximum in the summer hemisphere shifts to higher latitudes at higher altitudes and becomes comparable to and even larger than the winter peak. These features are consistent with the SABER analysis [*Ern et al.*, 2011]. It is also noted from both observations and the simulations that momentum fluxes decrease rapidly with altitude, indicating continuous

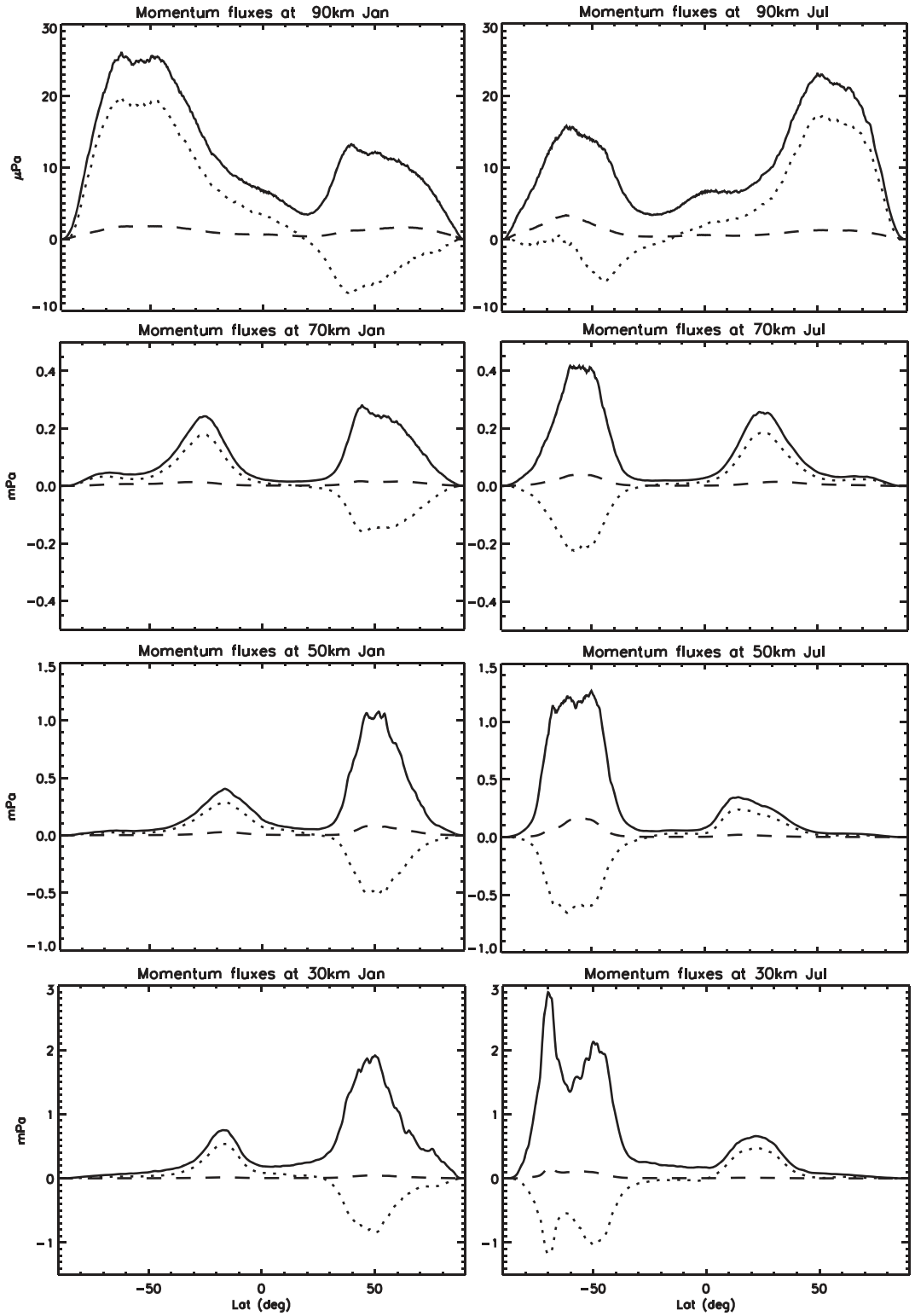

Figure 5. Zonal mean momentum flux averaged over (left column) January and (right column) July at 30, 50, 70, and 90 km, calculated from mesoscale-resolving WACCM. Solid lines: averages of absolute momentum flux, including both zonal and meridional components; dotted lines: averages of signed zonal momentum flux; dash line: averages of signed meridional momentum flux.

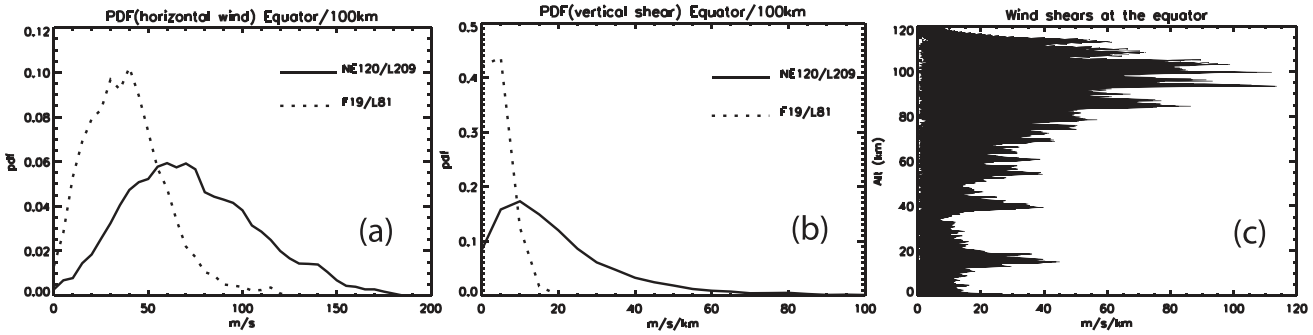

Figure 6. Probability density function (PDF) of (a) horizontal winds and (b) vertical shear of the horizontal winds at equatorial latitudes and ~100 km from the mesoscale-resolving WACCM (solid) and WACCM with ~2° horizontal resolution. (c) Vertical profiles of the vertical wind shears at equatorial latitudes from the mesoscale-resolving WACCM.

"peeling off" of the GW components with increasing altitudes. The MLT region is highly dynamic with shorter temporal and spatial scales and larger perturbation magnitudes compared with the lower atmosphere, which is consistent with the findings by *Koshyk et al.* [1999] and *Watanabe et al.* [2008] with regard to the vertical variation of energy spectra. The zonal forcing by resolved waves closes the jet in the summer mesosphere but at altitudes higher than climatology. In the winter mesosphere, the jet is slowed down but barely closed. It is thus still necessary to parameterize the forcing of GWs with scales smaller than 200 km. This is consistent with the findings by *Hamilton et al.* [1999] and *Siskind* [2014]. *Siskind* [2014] performed NOGAPS-ALPHA simulations with three different horizontal resolutions (T79, T239, and T479) and found that the vertical momentum fluxes increase significantly with spatial resolution (thus resolving greater fraction of GW spectrum), and the wave forcing does not yet converge at T479. As a result a cold bias at the winter stratopause and warm bias at the summer mesopause remain. It is not clear if a mesoscale-resolving whole atmosphere model with current GW parameterization schemes improves forecast skills over its coarse-resolution counterpart, but it is conceivable that with the wave spectrum to be parameterized being reduced by increasing resolution, the overall uncertainty and bias are reduced. The spatial and temporal variability are also better represented with increasing resolution.

As mentioned earlier, momentum deposition is one of the reasons why GWs are important for the upper atmosphere. Another reason is the large wave perturbations, which affect chemistry, dynamics, and electrodynamics. In the mesoscale-resolving WACCM simulations, although the resolved waves are still not sufficient for driving the observed circulation in the middle and upper atmosphere, the perturbations associated with these waves are much larger than those from coarser resolutions. Figures 6a and 6b are the probability density functions (PDFs) of horizontal winds and the vertical shear of these winds, respectively, in the equatorial lower thermosphere from the mesoscale-resolving WACCM simulations (solid lines) and those from ~2° resolution WACCM simulations (dotted lines). It is evident that the mesoscale-resolving simulation results have much larger dynamical ranges than the coarser resolution results. The vertical profiles of the shears (Figure 6c) at the equator show a clear maximum in the lower thermosphere with values exceeding 100ms^{-1} km^{-1}. The magnitude and the location of the large

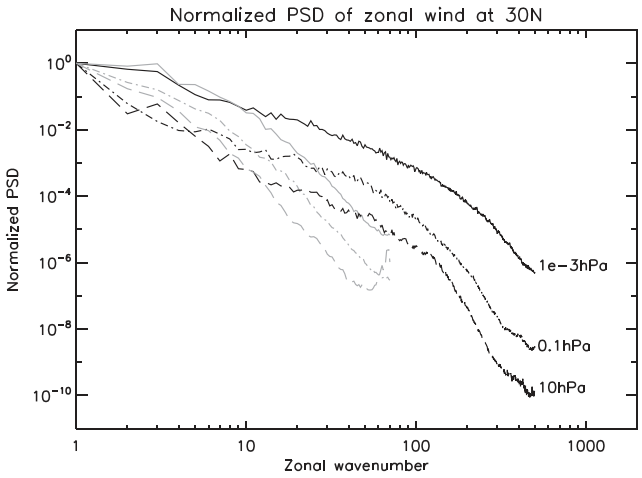

Figure 7. Power spectrum densities (PSDs) of zonal wind over zonal wave number in the stratosphere, mesosphere, and lower thermosphere from the mesoscale-resolving WACCM (black lines) and WACCM with ~2° horizontal resolution (gray lines). The PSDs have been normalized by their respective values at wave number 1.

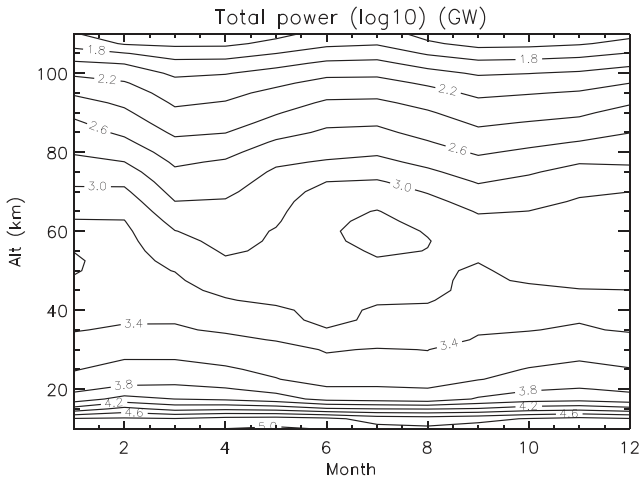

Figure 8. Monthly mean, globally integrated total wave flux of energy, including both pressure work and advection of kinetic energy, over 1year, calculated from mesoscale-resolving WACCM. Log10 scale is used, and the unit is Gigawatts (10^9 W).

shears are in good agreement with previous observations [*Larsen*, 2002] and could not be reproduced in coarser resolution models. As discussed earlier, the large winds and shears in the lower thermosphere have important implications for the stability, transport, and *E* region electrodynamics. By comparing the power spectrum densities from WACCM simulations from these two different resolutions (Figure 7), it is seen that the two generally agree at about zonal wave number 10 and lower at all three levels (the stratosphere, mesosphere, and lower thermosphere). At higher wave numbers, the power from ~2° resolution WACCM drops rapidly as compared to the mesoscale-resolving model. This suggests that ~2° resolution WACCM should be able to resolve most tidal waves and planetary waves, while processes with zonal scales of several thousand kilometers and less (including inertial gravity waves) will be underestimated. Due to the increasing significance of smaller-scale processes at higher altitudes, this underestimation becomes more severe in the MLT. From Figures 6 and 7 it is also clear that the smaller-scale processes are responsible for the large winds and shears in the MLT region.

Apart from controlling the MLT circulation and causing large perturbations in winds and shears, GWs can also affect thermospheric energetics. Figure 8 shows the monthly mean, globally integrated total wave energy flux (including both that due to pressure work and advection of kinetic energy) over a year, calculated from the mesoscale-resolving WACCM model. At 20 km, the total wave flux is between 4 and 7 × 10^{12} W (TW), and at 100 km the total power drops to 100–150 × 10^9 W (GW). The near-two-decade drop in energy flux is generally consistent with the change of gravity wave kinetic energy density as measured by *Balsley and Garello* [1985]. The energy flux in the lower thermosphere is comparable to the daily average Joule power input to the upper atmosphere [*Knipp et al.*, 2005]. Since the mesoscale-resolving WACCM does not capture the full wave spectrum, these values are likely underestimated by the model. It is also noted that the monthly mean total flux shows a semiannual cycle above the tropopause, with peaks in March and November in the stratosphere and January and July in the MLT.

These progresses of mesoscale-resolving global models in producing GWs features similar to observations are encouraging, though understanding, quantifying and forecasting ionosphere and thermosphere system down to mesoscales will remain to be a challenging problem. A mesoscale-resolving whole atmosphere model with self-consistent ionospheric electrodynamics is not yet available and will require significant computing resources. Idealized GWs and GWs from regional high-resolution models have been used to drive ionosphere and plasmasphere models [*Krall et al.*, 2013a, 2013b, *Hysell et al.*, 2014; *Wu et al.*, 2015], and it is found that GW wavelength and geometry, propagation direction with respect to the Earth magnetic field lines, spatial distribution, and their phase structure can affect the initiation of ESF. These findings suggest that the predictability of the GWs in the upper atmosphere have important implications for the predictability of ESF, and it will be important to explore what the effects are of a complex global wave system on the ionosphere and thermosphere system and how sensitive they are to different wave spectra.

The predictability of the upper atmosphere associated with mesoscale and GWs is a research area largely to be explored. Further progress will depend on better quantification of global GW distribution and temporal variability and better insights in the scale coupling and ion-neutral coupling. Novel development of numerical modeling, especially whole atmosphere modeling with mesh refinement capability, will provide valuable tools for the study. Lower and upper atmosphere observations can be assimilated into a whole atmosphere model to improve the specification and forecast of the upper atmosphere, as demonstrated by *Polavarapu et al.* [2005a], *Hoppel et al.* [2008], *Eckermann et al.* [2009], *Pedatella et al.* [2013, 2014b], and *Wang et al.* [2014].

However, whole atmosphere data assimilation also poses new challenges, as discussed by *Polavarapu et al.* [2005b], especially when mesoscale processes are better resolved. Adjustment during the assimilation step can generate spurious gravity waves, which albeit small locally [e.g., *Yamashita et al.*, 2010] can attain large amplitudes in the upper atmosphere. If not treated properly, such waves will likely degrade the forecast skills across scales in the upper atmosphere.

5. Summary

Statistical analysis of ionospheric observations suggested that lower atmosphere forcing can contribute significantly to its variability (up to ~35%), and observations, especially during the recent solar minimum, have provided further and more direct evidence of lower and upper atmosphere coupling. Numerical simulations with realistic lower atmosphere variability corroborate the statistical results and have been used to investigate pathways of the coupling and its implications for the predictability of the space environment.

Atmospheric tides can cause perturbations from the lower thermosphere/ionospheric *E* region up to the thermosphere and ionosphere *F* region. They can modulate the ionospheric wind dynamo by directly perturbing winds in the dynamo region. They also affect the neutral and plasma densities, both through direct wave perturbations, and by inducing transport between the mesosphere and thermosphere. Tidal perturbations of the neutral and plasma densities can affect the response of the thermosphere and ionosphere to the geomagnetic forcing. In addition to migrating components, nonmigrating tides and lunar tides are recognized to play an important role in the upper atmosphere.

Tides are highly variable with temporal scales ranging from day to day to interannual. Tidal variability is likely caused by a combination of variability of wave sources, propagation in and interaction with variable atmospheric wind and temperature structures, and nonlinear interaction among tides, planetary waves, and gravity waves. Numerical simulations of tidal variability associated with ENSO, QBO, and semiannual variations are consistent with observations. Short-term tidal (including lunar components) variability and their thermosphere and ionosphere impact, for example during SSW, have been quantified quite well in comparison with observations. Both observations and numerical models have shown that tides can change significantly from day to day. The day-to-day tidal variability is a ubiquitous feature, is more persistent, and has shorter time scales than suggested by tidal-planetary wave interactions. It appears to be stochastic and characterized by short autocorrelation time (a few days) and distance (tens of kilometers in the vertical direction). It may be related to the vacillation of the atmosphere system, though the exact causes and its implication for upper atmosphere predictability need further elucidation.

Planetary waves and equatorial waves may propagate up to the lower thermosphere and *E* region ionosphere. Like tides, they can impact the thermosphere and ionosphere system by affecting the transport between the mesosphere and thermosphere and perturbing the ionospheric *E* region dynamo. Generally, they cannot propagate beyond the lower thermosphere due to strong molecular dissipation (and also critical layer filtering), but tidal waves propagating deep into the thermosphere and ionospheric *F* region could be modulated by planetary waves-tidal interactions. Planetary waves have been shown to modulate vertical and meridional transport in the mesosphere and lower thermosphere.

Gravity waves become increasingly important in the upper atmosphere, because of their global presence, their increasing amplitudes with altitude, and their fast propagation speeds (which makes them less vulnerable to molecular dissipation). Dissipating gravity waves deposit momentum flux and affect the mean circulation and large-scale waves. They can induce wave and turbulent fluxes of heat and constituents and alter the thermal and compositional structures of the upper atmosphere. The large wave perturbations cause thermospheric and ionospheric disturbances (e.g., TADs and TIDs) and may seed ionospheric irregularities. Since they usually have spatial scales comparable to or smaller than the grid sizes of most global models, the gravity waves are poorly resolved or not resolved at all. The wave effects on the mean circulation and thermal and compositional structures have thus been parameterized in general circulation models and have been tuned to reproduce the observed climatology. The use of gravity wave parameterization is found to be a major source of model biases, given the simplifications and uncertainties of various schemes. The direct modulation of physical, chemical, and electrodynamical processes by mesoscale wave perturbations, on the other hand, are not accounted for in global models due to coarse model resolutions.

The apparent stochasticity of day-to-day tidal variability, probably resulting from the sensitive dependence of tides on the wave sources, propagation conditions, and nonlinear wave-wave and wave-mean flow interactions, along with model biases introduced by parameterized gravity wave forcing, poses challenges for quantifying and forecasting the upper atmosphere variability as related to the lower atmosphere forcing. To address these challenges, it is necessary to constrain the state of the whole atmosphere by assimilating observations of both the lower atmosphere and upper atmosphere. Better understanding and quantification of the gravity wave impacts on the upper atmosphere variability will depend on improving representation of mesoscale processes.

Acknowledgments

I would like to thank Delores Knipp for her invitation to write this review and numerous discussions with her in developing this paper. She read the first draft of the paper and provided valuable comments. I also thank Markus Rapp, who, as the Editor-in-Chief of *Journal of Atmospheric and Solar-Terrestrial Physics*, invited me to write a review paper on the subject of lower and upper atmosphere coupling back in 2010. Although I failed to fulfill the assignment (sorry, Markus Rapp), partly because back then I felt the connection between the lower atmosphere forcing and the ionosphere variability was still somewhat unclear in my mind, his invitation did provide me with the initiative. I would like to acknowledge the support of an international team (led by Larisa Goncharenko) by the International Space Science Institute (Bern, Switzerland) to collaborate on studying the coupling of the lower/upper atmosphere during stratospheric sudden warming. The review is in part based on a lecture given in 2015 at NCAR Advanced Study Program Summer Colloquia on Climate, Space Climate, and Couplings Between. I acknowledge high-performance computing support on Yellowstone (ark:/85065/d7wd3xhc) provided by NCAR's Computational and Information Systems Laboratory and from the NASA Advanced Supercomputing (NAS) Division at Ames Research Center provided by NASA High-End Computing (HEC) Program. Simulation outputs used to produce Figures 1, 2, and 5–8 are available upon request. Figures 3 and 4 have been properly cited and referred to in the reference list. The work is partially supported by National Science Foundation grant AGS-1138784 and AFOSRFA9550-16-1-0050. The National Center for Atmospheric Research is sponsored by the National Science Foundation.

References

Abdu, M. A., C. G. Brum, P. P. Batista, S. Gurubaran, D. Pancheva, J. V. Bageston, I. S. Batista, and H. Takahashi (2015), Fast and ultrafast Kelvin wave modulations of the equatorial evening *F* region vertical drift and spread *F* development, *Earth Planets Space*, *67*(1), 1–15, doi:10.1186/s40623-014-0143-5.

Akmaev, R., and G. Shved (1980), Modelling of the composition of the lower thermosphere taking account of the dynamics with applications to tidal variations of the [OI] 5577 å airglow, *J. Atmos. Terr. Phys.*, *42*, 705–716, doi:10.1016/0021-9169(80)90054-9.

Akmaev, R. A. (2011), Whole atmosphere modeling: Connecting terrestrial and space weather, *Rev. Geophys.*, *49*, RG4004, doi:10.1029/2011RG000364.

Akmaev, R. A., F. Wu, T. J. Fuller-Rowell, H. Wang, and M. D. Iredell (2010), Midnight density and temperature maxima, and thermospheric dynamics in Whole Atmosphere Model (WAM) simulations, *J. Geophys. Res.*, *115*, A08326, doi:10.1029/2010JA015651.

Alexander, M. J. (2015), Global and seasonal variations in three-dimensional gravity wave momentum flux from satellite limb-sounding temperatures, *Geophys. Res. Lett.*, *42*, 6860–6867, doi:10.1002/2015GL065234.

Alexander, M. J., and C. Barnet (2007), Using satellite observations to constrain gravity wave parameterizations for global models, *J. Atmos. Sci.*, *64*, 1652–1665.

Alexander, M. J., et al. (2008), Global estimates of gravity wave momentum flux from High Resolution Dynamics Limb Sounder observations, *J. Geophys. Res.*, *113*, D15S18, doi:10.1029/2007JD008807.

Alexander, M. J., et al. (2010), Recent developments in gravity-wave effects in climate models and the global distribution of gravity-wave momentum flux from observations and models, *Q. J. R. Meteorol. Soc.*, *136*, 1103–1124.

Altadill, D., and E. M. Apostolov (2001), Vertical propagating signatures of wave-type oscillations (2- and 6.5-days) in the ionosphere obtained from electron-density profiles, *J. Atmos. Terr. Phys.*, *63*, 823–834.

Andrews, D. G., J. R. Holton, and C. B. Leovy (1987), *Middle Atmosphere Dynamics*, 489 pp., Academic Press, Orlando, Fla.

Azeem, I., J. Yue, L. Hoffmann, S. D. Miller, W. C. Straka, and G. Crowley (2015), Multisensor profiling of a concentric gravity wave event propagating from the troposphere to the ionosphere, *Geophys. Res. Lett.*, *42*, 7874–7880, doi:10.1002/2015GL065903.

Bacmeister, J. T., M. F. Wehner, R. B. Neale, A. Gettelman, C. Hannay, P. H. Lauritzen, J. M. Caron, and J. E. Truesdale (2014), Exploratory high-resolution climate simulations using the Community Atmosphere Model (CAM), *J. Clim.*, *27*, 3073–3099, doi:10.1175/JCLI-D-13-00387.1.

Balsley, B. B., and R. Garello (1985), The kinetic energy density in the troposphere, stratosphere and mesosphere: A preliminary study using the Poker Flat MST radar in Alaska, *Radio Sci.*, *20*, 1355–1361.

Briggs, B. (1984), The variability of ionospheric dynamo currents, *J. Atmos. Terr. Phys.*, *46*(5), 419–429, doi:10.1016/0021-9169(84)90086-2.

Burrage, M. D., D. L. Wu, W. R. Skinner, D. A. Ortland, and P. B. Hays (1995), Latitude and seasonal dependence of the semidiurnal tide observed by the High-Resolution Doppler Imager, *J. Geophys. Res.*, *100*, 11,313–11,321.

Burrage, M. D., R. A. Vincent, H. G. Mayr, W. R. Skinner, N. F. Arnold, and P. B. Hays (1996), Long-term variability in the equatorial middle atmosphere zonal wind, *J. Geophys. Res.*, *101*, 12,847–12,854, doi:10.1029/96JD00575.

Chandran, A., R. R. Garcia, R. L. Collins, and L. C. Chang (2013), Secondary planetary waves in the middle and upper atmosphere following the stratospheric sudden warming event of January 2012, *Geophys. Res. Lett.*, *40*, 1861–1867, doi:10.1002/grl.50373.

Chang, L. C., S. E. Palo, and H.-L. Liu (2009), Short-term variation of the $s = 1$ nonmigrating semidiurnal tide during the 2002 sudden stratospheric warming, *J. Geophys. Res.*, *114*, D03109, doi:10.1029/2008JD010886.

Chang, L. C., S. E. Palo, and H.-L. Liu (2010), Response of the thermosphere and ionosphere to an ultra fast Kelvin wave, *J. Geophys. Res.*, *115*, A00G04, doi:10.1029/2010JA015453.

Chang, L. C., S. E. Palo, and H.-L. Liu (2011), Short-term variability in the migrating diurnal tide caused by interactions with the quasi 2 day wave, *J. Geophys. Res.*, *116*, D12112, doi:10.1029/2010JD014996.

Chang, L. C., J. Yue, W. Wang, Q. Wu, and R. R. Meier (2014), Quasi two day wave-related variability in the background dynamics and composition of the mesosphere/thermosphere and the ionosphere, *J. Geophys. Res. Space Physics*, *119*, 4786–4804, doi:10.1002/2014JA019936.

Charron, M., and E. Manzini (2002), Gravity waves from fronts: Parameterization and middle atmosphere response in a general circulation model, *J. Atmos. Sci.*, *59*, 923–941, doi:10.1175/1520-0469(2002)059<0923:GWFFPA>2.0.CO;2.

Chau, J. L., L. P. Goncharenko, B. G. Fejer, and H.-L. Liu (2012), Equatorial and low latitude ionospheric effects during sudden stratospheric warming events: Ionospheric effects during SSW events, *Space Sci. Rev.*, *168*, 385–417, doi:10.1007/s11214-011-9797-5.

Chau, J. L., P. Hoffmann, N. M. Pedatella, V. Matthias, and G. Stober (2015), Upper mesospheric lunar tides over middle and high latitudes during sudden stratospheric warming events, *J. Geophys. Res. Space Physics*, *120*, 3084–3096, doi:10.1002/2015JA020998.

Chen, P.-R. (1992), Two-day oscillation of the equatorial ionization anomaly, *J. Geophys. Res.*, *97*, 6343–6357.

Dewan, E. M., R. H. Picard, R. R. O'Neil, H. A. Gardiner, J. Gibson, J. D. Mill, E. Richards, M. Kendra, and W. O. Gallery (1998), MSX satellite observations of thunderstorm-generated gravity waves in mid-wave infrared images of the upper stratosphere, *Geophys. Res. Lett.*, *25*, 939–942, doi:10.1029/98GL00640.

Eckermann, S. D., and P. Preusse (1999), Global measurements of stratospheric mountain waves from space, *Science*, *286*, 1534–1537, doi:10.1126/science.286.5444.1534.

Eckermann, S. D., et al. (2009), High-altitude data assimilation system experiments for the northern summer mesosphere season of 2007, *J. Atmos. Sol. Terr. Phys.*, *71*, 531–551, doi:10.1016/j.jastp.2008.09.036.

Ern, M., P. Preusse, M. J. Alexander, and C. D. Warner (2004), Absolute values of gravity wave momentum flux derived from satellite data, *J. Geophys. Res.*, *109*, D20103, doi:10.1029/2004JD004752.

Ern, M., P. Preusse, J. C. Gille, C. L. Hepplewhite, M. G. Mlynczak, J. M. R. III, and M. Riese (2011), Implications for atmospheric dynamics derived from global observations of gravity wave momentum flux in stratosphere and mesosphere, *J. Geophys. Res.*, *116*, D19107, doi:10.1029/2011JD015821.

Fang, T.-W., R. Akmaev, T. Fuller-Rowell, F. Wu, N. Maruyama, and G. Millward (2013), Longitudinal and day-to-day variability in the ionosphere from lower atmosphere tidal forcing, *Geophys. Res. Lett.*, *40*, 2523–2528, doi:10.1002/grl.50550.

Fejer, B. G., M. E. Olson, J. L. Chau, C. Stolle, H. Lühr, L. P. Goncharenko, K. Yumoto, and T. Nagatsuma (2010), Lunar-dependent equatorial ionospheric electrodynamic effects during sudden stratospheric warmings, *J. Geophys. Res.*, *115*, A00G03, doi:10.1029/2010JA015273.

Fejer, B. G., B. D. Tracy, M. E. Olson, and J. L. Chau (2011), Enhanced lunar semidiurnal equatorial vertical plasma drifts during sudden stratospheric warmings, *Geophys. Res. Lett.*, *39*, L21104, doi:10.1029/2011GL049788.

Fetzer, E. J., and J. C. Gille (1994), Gravity wave variance in LIMS temperatures. Part I: Variability and comparison with background winds, *J. Atmos. Sci.*, *51*, 2461–2483.

Forbes, J. M. (1995), Tidal and planetary waves, in *The Upper Mesosphere and Lower Thermosphere: A Review of Experiment and Theory*, Geophys. Monogr. Ser., edited by R. M. Johnson and T. L. Killeen, p. 356, AGU, Washington, D. C.

Forbes, J. M., and R. S. Lindzen (1976), Atmospheric solar tides and their electrodynamic effects: I. The global Sq current system, *J. Atmos. Terr. Phys.*, *38*, 897–910.

Forbes, J. M., and Y. Moudden (2012), Quasi-two-day wave-tide interactions as revealed in satellite observations, *J. Geophys. Res.*, *117*, D12110, doi:10.1029/2011JD017114.

Forbes, J. M., and R. A. Vincent (1989), Effects of mean winds and dissipation on the diurnal propagating tide: An analytic approach, *Planet. Space Sci.*, *37*, 197–209, doi:10.1016/0032-0633(89)90007-X.

Forbes, J. M., and X. Zhang (2012), Lunar tide amplification during the January 2009 stratosphere warming event: Observations and theory, *J. Geophys. Res.*, *117*, A12312, doi:10.1029/2012JA017963.

Forbes, J. M., R. G. Roble, and C. G. Fesen (1993), Acceleration, heating, and compositional mixing of the thermosphere due to upward propagating tides, *J. Geophys. Res.*, *98*, 311–321, doi:10.1029/92JA00442.

Forbes, J. M., S. Palo, and X. Zhang (2000), Variability of the ionosphere, *J. Atmos. Sol. Terr. Phys.*, *62*, 685–693.

Forbes, J. M., X. Zhang, S. Palo, J. Russell, C. J. Mertens, and M. Mlynczak (2008), Tidal variability in the ionospheric dynamo region, *J. Geophys. Res.*, *113*, A02310, doi:10.1029/2007JA012737.

Forbes, J. M., S. L. Bruinsma, X. Zhang, and J. Oberheide (2009), Surface-exosphere coupling due to thermal tides, *Geophys. Res. Lett.*, *36*, L15812, doi:10.1029/2009GL038748.

Fritts, D. C., and M. J. Alexander (2003), Gravity wave dynamics and effects in the middle atmosphere, *Rev. Geophys.*, *41*, 1003, doi:10.1029/2001RG000106.

Fritts, D. C., et al. (2016), The Deep Propagating Gravity Wave Experiment (DEEPWAVE): An airborne and ground-based exploration of gravity wave propagation and effects from their sources throughout the lower and middle atmosphere, *Bull. Am. Meteorol. Soc.*, *97*, 425–453, doi:10.1175/BAMS-D-14-00269.1.

Fuller-Rowell, T. J., F. Wu, R. A. Akmaev, and E. Araujo-Pradere (2010), A whole atmosphere model simulation of the impact of a sudden stratospheric warming on thermosphere dynamics and electrodynamics, *J. Geophys. Res.*, *115*, A00G08, doi:10.1029/2010JA015524.

Fuller-Rowell, T. J., H. Wang, R. A. Akmaev, F. Wu, T.-W. Fang, M. Iredell, and A. D. Richmond (2011), Forecasting the dynamic and electrodynamic response to the January 2009 sudden stratospheric warming, *Geophys. Res. Lett.*, *38*, L13102, doi:10.1029/2011GL047732.

Gan, Q., J. Yue, L. C. Chang, W. B. Wang, S. D. Zhang, and J. Du (2015), Observations of thermosphere and ionosphere changes due to the dissipative 6.5-day wave in the lower thermosphere, *Ann. Geophys.*, *33*(7), 913–922, doi:10.5194/angeo-33-913-2015.

Garcia, R. R., R. Lieberman, J. M. R. III, and M. G. Mlynczak (2005), Large-scale waves in the mesosphere and lower thermosphere observed by SABER, *J. Atmos. Sci.*, *62*(12), 4384–4399, doi:10.1175/JAS3612.1.

Garcia, R. R., D. R. Marsh, D. E. Kinnison, B. A. Boville, and F. Sassi (2007), Simulation of secular trends in the middle atmosphere, 1950–2003, *J. Geophys. Res.*, *112*, D09301, doi:10.1029/2006JD007485.

Gasperini, F., J. M. Forbes, E. N. Doornbos, and S. L. Bruinsma (2015), Wave coupling between the lower and middle thermosphere as viewed from TIMED and GOCE, *J. Geophys. Res. Space Physics*, *120*, 5788–5804, doi:10.1002/2015JA021300.

Geller, M. A., et al. (2013), A comparison between gravity wave momentum fluxes in observations and climate models, *J. Clim.*, *26*, 6383–6405, doi:10.1175/JCLI-D-12-00545.1.

Goncharenko, L., J. Chau, H.-L. Liu, and A. J. Coster (2010), Unexpected connections between the stratosphere and ionosphere, *Geophys. Res. Lett.*, *37*, L10101, doi:10.1029/2010GL043125.

Gong, J., and M. A. Geller (2010), Vertical fluctuation energy in United States high vertical resolution radiosonde data as an indicator of convective gravity wave sources, *J. Geophys. Res.*, *115*, D11110, doi:10.1029/2009JD012265.

Gong, J., D. L. Wu, and S. D. Eckermann (2012), Gravity wave variances and propagation derived from AIRS radiances, *Atmos. Chem. Phys.*, *12*(4), 1701–1720, doi:10.5194/acp-12-1701-2012.

Gray, L. J., S. Sparrow, M. Juckes, A. O'Neill, and D. G. Andrews (2003), Flow regimes in the winter stratosphere of the Northern Hemisphere, *Q. J. R. Meteorol. Soc.*, *129*, 925–945, doi:10.1256/qj.02.82.

Gu, S.-Y., H.-L. Liu, T. Li, X. Dou, Q. Wu, and J. M. Russell (2014), Observation of the neutral-ion coupling through 6-day planetary wave, *J. Geophys. Res. Space Physics*, *119*, 10,376–10,383, doi:10.1002/2014JA020530.

Gu, S.-Y., H.-L. Liu, T. Li, X. Dou, Q. Wu, and J. M. Russell (2015), Evidence of nonlinear interaction between quasi 2-day wave and quasi-stationary wave, *J. Geophys. Res. Space Physics*, *120*, 1256–1263, doi:10.1002/2014JA020919.

Gu, S.-Y., H.-L. Liu, N. M. Pedatella, X. Dou, T. Li, and T. Chen (2016), The quasi 2-day wave activities during 2007 austral summer period as revealed by whole atmosphere community climate model, *J. Geophys. Res. Space Physics*, doi:10.1002/2015JA022225.

Hagan, M. E., M. D. Burrage, J. M. Forbes, J. Hackney, W. J. Randel, and X. Zhang (1999), GSWM-98: Results for migrating solar tides, *J. Geophys. Res.*, *104*, 6813–6828.

Hagan, M. E., A. Maute, R. G. Roble, A. D. Richmond, T. J. Immel, and S. L. England (2007), Connections between deep tropical clouds and the Earth's ionosphere, *Geophys. Res. Lett.*, *34*, L20109, doi:10.1029/2007GL030142.

Haldoupis, C. (2012), Midlatitude sporadic *E*. A typical paradigm of atmosphere-ionosphere coupling, *Space Sci. Rev.*, *168*, 441–461, doi:10.1007/s11214-011-9786-8.

Hamilton, K., R. J. Wilson, and R. S. Hemler (1999), Middle atmosphere simulated with high vertical and horizontal resolution versions of a GCM: Improvements in the cold pole bias and generation of a QBO-like oscillation in the tropics, *J. Atmos. Sci.*, *56*, 3829–3846.

Harris, T. J., and R. A. Vincent (1993), The quasi-two-day wave observed in the equatorial middle atmosphere, *J. Geophys. Res.*, *98*, 10,481–10,490, doi:10.1029/93JD00380.

Häusler, K., and H. Lühr (2009), Nonmigrating tidal signals in the upper thermospheric zonal wind at equatorial latitudes as observed by CHAMP, *Ann. Geophys.*, *27*, 2643–2652.

Häusler, K., H. Lühr, S. Rentz, and W. Köhler (2007), A statistical analysis of longitudinal dependences of upper thermospheric zonal winds at dip equator latitudes derived from CHAMP, *J. Atmos. Sol. Terr. Phys.*, *69*, 1419–1430, doi:10.1016/j.jastp.2007.04.004.
Häusler, K., H. Lühr, M. E. Hagan, A. Maute, and R. G. Roble (2010), Comparison of CHAMP and TIME-GCM nonmigrating tidal signals in the thermospheric zonal wind, *J. Geophys. Res.*, *115*, D00I08, doi:10.1029/2009JD012394.
Hecht, J. H., R. L. Walterscheid, L. J. Gelinas, R. A. Vincent, I. M. Reid, and J. M. Woithe (2010), Observations of the phase-locked 2 day wave over the Australian sector using medium-frequency radar and airglow data, *J. Geophys. Res.*, *115*, D16115, doi:10.1029/2009JD013772.
Hertzog, A., G. Boccara, R. A. Vincent, F. Vial, and P. Cocquerez (2008), Estimation of gravity wave momentum flux and phase speeds from quasi-Lagrangian stratospheric balloon flights. Part II: Results from the Vorcore campaign in Antarctica, *J. Atmos. Sci.*, *65*, 3056–3070, doi:10.1175/2008JAS2710.1.
Hickey, M. P., G. Schubert, and R. L. Walterscheid (2001), Acoustic wave heating of the thermosphere, *J. Geophys. Res.*, *106*, 21,543–21,548, doi:10.1029/2001JA000036.
Hines, C. O. (1960), Internal atmospheric gravity waves at ionospheric heights, *Can. J. Phys*, *38*, 1441–1481.
Hirota, I., and T. Hirooka (1984), Normal mode Rossby waves observed in the upper stratosphere, Part 1: First symmetric modes of zonal wavenumbers 1 and 2, *J. Atmos. Sci.*, *41*, 1253–1267.
Hoffmann, L., and M. J. Alexander (2009), Retrieval of stratospheric temperatures from atmospheric infrared sounder radiance measurements for gravity wave studies, *J. Geophys. Res.*, *114*, D07105, doi:10.1029/2008JD011241.
Holton, J. R., and C. Mass (1976), Stratospheric vacillation cycles, *J. Atmos. Sci.*, *33*, 2218–2225.
Hoppel, K. W., N. L. Baker, L. Coy, S. D. Eckermann, J. P. McCormack, G. E. Nedoluha, and D. E. Siskind (2008), Assimilation of stratospheric and mesospheric temperatures from MLS and SABER into a global NWP model, *Atmos. Chem. Phys.*, *8*, 6103–6116, doi:10.5194/acp-8-6103-2008.
Huba, J. D., D. P. Drob, T.-W. Wu, and J. J. Makela (2015), Modeling the ionospheric impact of tsunami-driven gravity waves with SAMI3: Conjugate effects, *Geophys. Res. Lett.*, *42*, 5719–5726, doi:10.1002/2015GL064871.
Hysell, D. L., R. Jafari, M. A. Milla, and J. W. Meriwether (2014), Data-driven numerical simulations of equatorial spread *F* in the Peruvian sector, *J. Geophys. Res. Space Physics*, *119*, 3815–3827, doi:10.1002/2014JA019889.
Immel, T. J., E. Sagawa, S. L. England, S. B. Henderson, M. E. Hagan, S. B. Mende, H. U. Frey, C. M. Swenson, and L. J. Paxton (2006), Control of equatorial ionospheric morphology by atmospheric tides, *Geophys. Res. Lett.*, *33*, L15108, doi:10.1029/2006GL026161.
Jin, H., Y. Miyoshi, D. Pancheva, P. Mukhtarov, H. Fujiwara, and H. Shinagawa (2012), Response of migrating tides to the stratospheric sudden warming in 2009 and their effects on the ionosphere studied by a whole atmosphere-ionosphere model GAIA with COSMIC and TIMED/SABER observations, *J. Geophys. Res.*, *117*, A10323, doi:10.1029/2012JA017650.
Jones, M., J. M. Forbes, M. E. Hagan, and A. Maute (2014), Impacts of vertically propagating tides on the mean state of the ionosphere-thermosphere system, *J. Geophys. Res. Space Physics*, *119*, 2197–2213, doi:10.1002/2013JA019744.
Jung, T., et al. (2012), High-resolution global climate simulations with the ECMWF model in Project Athena: Experimental design, model climate, and seasonal forecast skill, *J. Clim.*, *25*(9), 3155–3172, doi:10.1175/JCLI-D-11-00265.1.
Kalisch, S., P. Preusse, M. Ern, S. D. Eckermann, and M. Riese (2014), Differences in gravity wave drag between realistic oblique and assumed vertical propagation, *J. Geophys. Res. Atmos.*, *119*, 10,081–10,099, doi:10.1002/2014JD021779.
Kalnay, E. (2003), *Atmospheric Modeling, Data Assimilation and Predictability*, 341 pp., Cambridge Univ. Press, Cambridge, U. K.
Kelley, M. C., M. F. Larsen, C. LaHoz, and J. P. McClure (1981), Gravity wave initiation of equatorial spread *F*: A case study, *J. Geophys. Res.*, *86*, 9087–9100, doi:10.1029/JA086iA11p09087.
Knipp, D. J., W. K. Tobiska, and B. A. Emery (2005), Direct and indirect thermospheric heating sources for solar cycles 21–23, *Sol. Phys.*, *224*, 495–505, doi:10.1007/s11207-005-6393-4.
Koshyk, J. N., B. A. Boville, K. Hamilton, E. Manzini, and K. Shibata (1999), Kinetic energy spectrum of horizontal motions in middle-atmosphere models, *J. Geophys. Res.*, *104*, 27,177–27,190.
Krall, J., J. D. Huba, and D. C. Fritts (2013a), On the seeding of equatorial spread *F* by gravity waves, *Geophys. Res. Lett.*, *40*, 661–664, doi:10.1002/grl.50144.
Krall, J., J. D. Huba, G. Joyce, and M. Hei (2013b), Simulation of the seeding of equatorial spread F by circular gravity waves, *Geophys. Res. Lett.*, *40*, 1–5, doi:10.1029/2012GL054022.
Larsen, M. F. (2002), Winds and shears in the mesosphere and lower thermosphere: Results from four decades of chemical release wind measurements, *J. Geophys. Res.*, *107*, 1215, doi:10.1029/2001JA000218.
Laštovička, J. (2006), Forcing of the ionosphere by waves from below, *J. Atmos. Sol. Terr. Phys.*, *68*(3–5), 479–497, doi:10.1016/j.jastp.2005.01.018.
Lean, H. W., P. A. Clark, M. Dixon, N. M. Roberts, A. Fitch, R. Forbes, and C. Halliwell (2008), Characteristics of high-resolution versions of the Met Office unified model for forecasting convection over the United Kingdom, *Mon. Weather Rev.*, *136*(9), 3408–3424, doi:10.1175/2008MWR2332.1.
Lei, J., J. M. Forbes, H. L. Liu, X. Dou, X. Xue, T. Li, and X. Luan (2011), Latitudinal variations of middle thermosphere: Observations and modeling, *J. Geophys. Res.*, *116*, A12306, doi:10.1029/2011JA017067.
Lei, J., J. P. Thayer, W. Wang, J. Yue, and X. Dou (2014), Nonmigrating tidal modulation of the equatorial thermosphere and ionosphere anomaly, *J. Geophys. Res. Space Physics*, *119*, 3036–3043, doi:10.1002/2013JA019749.
Lieberman, R. S., and D. Riggin (1997), High resolution Doppler imager observations of Kelvin waves in the equatorial mesosphere and lower thermosphere, *J. Geophys. Res.*, *102*, 26,117–26,130, doi:10.1029/96JD02902.
Lieberman, R. S., D. M. Riggin, S. J. Franke, A. H. Manson, C. M. T. Nakamura, T. Tsuda, R. A. Vincent, and I. Reid (2003), The 6.5-day wave in the mesosphere and lower thermosphere: Evidence for baroclinic/barotropic instability, *J. Geophys. Res.*, *108*, 4640, doi:10.1029/2002JD003349.
Lieberman, R. S., D. M. Riggin, D. A. Ortland, S. W. Nesbitt, and R. A. Vincent (2007), Variability of mesospheric diurnal tides and tropospheric diurnal heating during 1997–1998, *J. Geophys. Res.*, *112*, D20110, doi:10.1029/2007JD008578.
Liu, H.-L. (2014), WACCM-X simulation of upper atmosphere wave variability, in *Modeling the Ionosphere and Thermosphere System, Geophys. Monogr. Ser.,* chap. 16, edited by J. Huba, R. Schunk, and G. Khazanov, pp. 181–200, AGU, Washington, D. C., doi:10.1002/9781118704417.ch16.
Liu, H.-L., and M. E. Hagan (1998), Local heating/cooling of the mesosphere due to gravity wave and tidal coupling, *Geophys. Res. Lett.*, *25*, 2941–2944.
Liu, H.-L., and A. D. Richmond (2013), Attribution of ionospheric vertical plasma drift perturbations to large-scale waves and the dependence on solar activity, *J. Geophys. Res. Space Physics*, *118*, 2452–2465, doi:10.1002/jgra.50265.
Liu, H.-L., and R. G. Roble (2002), A study of a self-generated stratospheric sudden warming and its mesospheric/lower thermospheric impacts using coupled TIME-GCM/CCM3, *J. Geophys. Res.*, *107*, 4695, doi:10.1029/2001JD001533.

Liu, H.-L., and S. L. Vadas (2013), Large-scale ionospheric disturbances due to the dissipation of convectively-generated gravity waves over Brazil, *J. Geophys. Res.*, 2419–2427, doi:10.1002/jgra.50244.
Liu, H.-L., M. E. Hagan, and R. G. Roble (2000), Local mean state changes due to gravity wave breaking modulated by diurnal tide, *J. Geophys. Res.*, *105*, 12,381–12,396.
Liu, H.-L., E. R. Talaat, R. G. Roble, R. S. Lieberman, D. M. Riggin, and J.-H. Yee (2004), 6.5-day wave and its seasonal variability in the middle and upper atmosphere, *J. Geophys. Res.*, *109*, D21112, doi:10.1029/2004JD004795.
Liu, H.-L., F. Sassi, and R. R. Garcia (2009), Error growth in a whole atmosphere climate model, *J. Atmos. Sci.*, *66*, 173–186.
Liu, H.-L., W. Wang, A. D. Richmond, and R. G. Roble (2010a), Ionospheric variability due to planetary waves and tides for solar minimum conditions, *J. Geophys. Res.*, *115*, A00G01, doi:10.1029/2009JA015188.
Liu, H.-L., V. A. Yudin, and R. G. Roble (2013), Day-to-day ionospheric variability due to lower atmosphere perturbations, *Geophys. Res. Lett.*, *40*, 1–6, doi:10.1002/grl.50125.
Liu, H.-L., J. M. McInerney, S. Santos, P. H. Lauritzen, M. A. Taylor, and N. M. Pedatella (2014a), Gravity waves simulated by high-resolution Whole Atmosphere Community Climate Model, *Geophys. Res. Lett.*, *41*, 9106–9112, doi:10.1002/2014GL062468.
Liu, H. L., et al. (2007), Comparative study of short term tidal variability, *J. Geophys. Res.*, *112*, D18108, doi:10.1029/2007JD008542.
Liu, H.-L., et al. (2010b), Thermosphere extension of the Whole Atmosphere Community Climate Model, *J. Geophys. Res.*, *115*, A12302, doi:10.1029/2010JA015586.
Liu, X., J. Xu, J. Yue, H. L. Liu, and W. Yuan (2014b), Large winds and wind shears caused by the nonlinear interactions between gravity waves and tidal backgrounds in the mesosphere and lower thermosphere, *J. Geophys. Res. Space Physics*, *119*, 7698–7708, doi:10.1002/2014JA020221.
Lorenz, E. N. (1963), Deterministic nonperiodic flow, *J. Atmos. Sci.*, *20*, 130–141.
Lorenz, E. N. (1969), Atmospheric predictability as revealed by naturally occurring analogues, *J. Atmos. Sci.*, *26*, 636–646.
Lühr, H., M. Rother, K. Häusler, P. Alken, and S. Maus (2008), The influence of nonmigrating tides on the longitudinal variation of the equatorial electrojet, *J. Geophys. Res.*, *113*, A08313, doi:10.1029/2008JA013064.
Manzini, E., M. A. Giorgetta, M. Esch, L. Kornblueh, and E. Roeckner (2006), The influence of sea surface temperatures on the northern winter stratosphere: Ensemble simulations with the MAECHAM5 model, *J. Clim.*, *19*, 3863–3881.
Mathews, J. (1998), Sporadic *E*: Current views and recent progress, *J. Atmos. Sol. Terr. Phys.*, *60*, 413–435, doi:10.1016/S1364-6826(97)00043-6.
Matsuno, T. (1971), A dynamical model of the stratospheric sudden warming, *J. Atmos. Sci.*, *28*, 1479–1494.
Matthias, V., T. G. Shepherd, P. Hoffmann, and M. Rapp (2015), The Hiccup: A dynamical coupling process during the autumn transition in the Northern Hemisphere – Similarities and differences to sudden stratospheric warmings, *Ann. Geophys.*, *33*(2), 199–206, doi:10.5194/angeo-33-199-2015.
McCormack, J. P., L. Coy, and K. W. Hoppel (2009), Evolution of the quasi 2-day wave during January 2006, *J. Geophys. Res.*, *114*, D20115, doi:10.1029/2009JD012239.
McLandress, C. (1998), On the importance of gravity waves in the middle atmosphere and their parameterization in general circulation models, *J. Atmos. Sol. Terr. Phys.*, *60*, 1357–1383, doi:10.1016/S1364-6826(98)00061-3.
McLandress, C. M. (2002), The seasonal variation of the propagating diurnal tide in the mesosphere and lower thermosphere. Part II: The role of tidal heating and zonal mean winds, *J. Atmos. Sci.*, *59*, 907–922.
Meng, X., A. Komjathy, O. P. Verkhoglyadova, Y.-M. Yang, Y. Deng, and A. J. Mannucci (2015), A new physics-based modeling approach for tsunami-ionosphere coupling, *Geophys. Res. Lett.*, *42*, 4736–4744, doi:10.1002/2015GL064610.
Meyer, C. K., and J. M. Forbes (1997), A 6.5-day westward propagating planetary wave: Origin and characteristics, *J. Geophys. Res.*, *102*, 26,173–26,178.
Miller, S. D., W. C. Straka, J. Yue, S. M. Smith, M. J. Alexander, L. Hoffmann, M. Setvák, and P. T. Partain (2015), Upper atmospheric gravity wave details revealed in nightglow satellite imagery, *Proc. Natl. Acad. Sci.*, *112*(49), E6728–E6735, doi:10.1073/pnas.1508084112.
Millward, G. H., I. Müller-Wodarg, A. Aylward, T. Fuller-Rowell, A. Richmond, and R. Moffett (2001), An investigation into the influence of tidal forcing on *F* region equatorial vertical ion drift using a global ionosphere-thermosphere model with coupled electrodynamics, *J. Geophys. Res.*, *106*, 24,733–24,744.
Miyoshi, Y., H. Fujiwara, J. M. Forbes, and S. L. Bruinsma (2009), Solar terminator wave and its relation to the atmospheric tide, *J. Geophys. Res.*, *114*, A07303, doi:10.1029/2009JA014110.
Miyoshi, Y., H. Fujiwara, H. Jin, and H. Shinagawa (2014), A global view of gravity waves in the thermosphere simulated by a general circulation model, *J. Geophys. Res. Space Physics*, *119*, 5807–5820, doi:10.1002/2014JA019848.
Miyoshi, Y., H. Fujiwara, H. Jin, and H. Shinagawa (2015), Impacts of sudden stratospheric warming on general circulation of the thermosphere, *J. Geophys. Res. Space Physics*, *120*, 10,897–10,912, doi:10.1002/2015JA021894.
Moudden, Y., and J. M. Forbes (2014), Quasi-two-day wave structure, interannual variability, and tidal interactions during the 2002–2011 decade, *J. Geophys. Res. Atmospheres*, *119*, 2241–2260, doi:10.1002/2013JD020563.
Muller, H., and L. Nelson (1978), A travelling quasi 2-day wave in the meteor region, *J. Atmos. Terr. Phys.*, *40*, 761–766, doi:10.1016/0021-9169(78)90136-8.
Müller-Wodarg, I., and A. Aylward (1998), The influence of tides on composition of the thermosphere, *Adv. Space Res.*, *21*, 807–810, doi:10.1016/S0273-1177(97)00678-9.
Ngan, K., and G. E. Eperon (2012), Middle atmosphere predictability in a numerical weather prediction model: Revisiting the inverse error cascade, *Q. J. R. Meteorol. Soc.*, *138*, 1366–1378, doi:10.1002/qj.984.
Nishioka, M., T. Tsugawa, M. Kubota, and M. Ishii (2013), Concentric waves and short-period oscillations observed in the ionosphere after the 2013 Moore EF5 tornado, *Geophys. Res. Lett.*, *40*, 5581–5586, doi:10.1002/2013GL057963.
Oberheide, J., J. M. Forbes, K. Häusler, Q. Wu, and S. L. Bruinsma (2009), Tropospheric tides from 80 to 400 km: Propagation, interannual variability, and solar cycle effects, *J. Geophys. Res.*, *114*, D00I05, doi:10.1029/2009JD012388.
Ortland, D. A., and M. J. Alexander (2006), Gravity wave influence on the global structure of the diurnal tide in the mesosphere and lower thermosphere, *J. Geophys. Res.*, *111*, A10S10, doi:10.1029/2005JA011467.
Palo, S. E., R. G. Roble, and M. E. Hagan (1999), Middle atmosphere effects of the quasi-two-day wave determined from a general circulation model, *Earth Planets Space*, *51*, 629–647.
Pancheva, D., P. Mukhtarov, and B. Andonov (2009), Nonmigrating tidal activity related to the sudden stratospheric warming in the Arctic winter of 2003/2004, *Ann. Geophys.*, *27*(3), 975–987, doi:10.5194/angeo-27-975-2009.
Pancheva, D., et al. (2008), Planetary wave coupling (5–6-day waves) in the low-latitude atmosphere-ionosphere system, *J. Atmos. Sol. Terr. Phys.*, *70*, 101–122, doi:10.1016/j.jastp.2007.10.003.

Pancheva, D. V. (2006), Quasi-2-day wave and tidal variability observed over Ascension Island during January/February 2003, *J. Atmos. Sol. Terr. Phys.*, *68*, 390–407.
Pancheva, D. V., et al. (2006), Two-day wave coupling of the low-latitude atmosphere-ionosphere system, *J. Geophys. Res.*, *111*, A07313, doi:10.1029/2005JA011562.
Park, J., H. Lühr, M. Kunze, B. G. Fejer, and K. W. Min (2012), Effect of sudden stratospheric warming on lunar tidal modulation of the equatorial electrojet, *J. Geophys. Res.*, *117*, A03306, doi:10.1029/2011JA017351.
Pedatella, N., H.-L. Liu, F. Sassi, J. Lei, J. Chau, and X. Zhang (2014a), Ionosphere variability during the 2009 SSW: Influence of the lunar semidiurnal tide and mechanisms producing electron density variability, *J. Geophys. Res. Space Physics*, *119*, 3828–3843, doi:10.1002/2014JA019849.
Pedatella, N. M., and H.-L. Liu (2012), Tidal variability in the mesosphere and lower thermosphere due to the El Niño/Southern Oscillation, *Geophys. Res. Lett.*, *39*, L19802, doi:10.1029/2012GL053383.
Pedatella, N. M., and H.-L. Liu (2013), Influence of the El Niño Southern Oscillation on the middle and upper atmosphere, *J. Geophys. Res. Space Physics*, *118*, 2744–2755, doi:10.1002/jgra.50286.
Pedatella, N. M., H.-L. Liu, and M. E. Hagan (2012), Day-to-day migrating and nonmigrating tidal variability due to the six-day planetary wave, *J. Geophys. Res.*, *117*, A06301, doi:10.1029/2012JA017581.
Pedatella, N. M., K. Raeder, J. L. Anderson, and H.-L. Liu (2013), Application of data assimilation in the whole atmosphere community climate model to the study of day-to-day variability in the middle and upper atmosphere, *Geophys. Res. Lett.*, *40*, 4469–4474, doi:10.1002/grl.50884.
Pedatella, N. M., K. Raeder, J. L. Anderson, and H.-L. Liu (2014b), Ensemble data assimilation in the whole atmosphere community climate model, *J. Geophys. Res. Atmos.*, *119*, 9793–9809, doi:10.1002/2014JD021776.
Pedatella, N. M., A. D. Richmond, A. Maute, and H.-L. Liu (2016), Impact of semidiurnal tidal variability during SSWs on the mean state of the ionosphere and thermosphere, *J. Geophys. Res. Space Physics*, *121*, doi:10.1002/2016JA022910.
Pedatella, N. M., et al. (2014c), The neutral dynamics during the 2009 sudden stratosphere warming simulated by different whole atmosphere models, *J. Geophys. Res.*, *119*, 1306–1324, doi:10.1002/2013JA019421.
Phillips, A., and B. Briggs (1991), The day-to-day variability of upper atmosphere tidal winds and dynamo currents, *J. Atmos. Terr. Phys.*, *53*, 39–47, doi:10.1016/0021-9169(91)90018-3.
Plumb, R. A. (1983), Baroclinic instability of the summer mesosphere: A mechanism for the quasi-two-day wave?, *J. Atmos. Sci.*, *40*, 262–270.
Polavarapu, S., S. Ren, Y. Rochon, D. Sankey, N. Ek, J. Koshyk, and D. Tarasick (2005a), Data assimilation with the Canadian Middle Atmosphere Model, *Atmos. Ocean*, *43*, 77–100, doi:10.3137/ao.430105.
Polavarapu, S., T. G. Shepherd, Y. ROCHON, and S. REN (2005b), Some challenges of middle atmosphere data assimilation, *Q. J. R. Meteorol. Soc.*, *131*, 3513–3527, doi:10.1256/qj.05.87.
Richmond, A. D., and R. G. Roble (1987), Electrodynamic effects of thermospheric winds from the NCAR Thermospheric General-Circulation Model, *J. Geophys. Res.*, *92*, 12,365–12,376.
Richmond, A. D., S. Matsushita, and J. D. Tarpley (1976), On the production mechanism of electric currents and fields in the ionosphere, *J. Geophys. Res.*, *81*, 547–555, doi:10.1029/JA081i004p00547.
Richter, J. H., F. Sassi, and R. R. Garcia (2010), Toward a physically based gravity wave source parameterization in a general circulation model, *J. Atmos. Sci.*, *67*, 136–156, doi:10.1175/2009JAS3112.1.
Rishbeth, H., and M. Mendillo (2001), Patterns of ionospheric variability, *J. Atmos. Solar Terr. Phys.*, *63*, 1661–1680.
Rodgers, C. D., and A. J. Prata (1981), Evidence for a traveling two-day wave in the middle atmosphere, *J. Geophys. Res.*, *86*, 9661–9664, doi:10.1029/JC086iC10p09661.
Ruan, H., J. Lei, X. Dou, W. Wan, and Y. Liu (2014), Midnight density maximum in the thermosphere from the CHAMP observations, *J. Geophys. Res. Space Physics*, *119*, 3741–3746, doi:10.1002/2013JA019566.
Sagawa, E., T. J. Immel, H. U. Frey, and S. B. Mende (2005), Longitudinal structure of the equatorial anomaly in the nighttime ionosphere observed by IMAGE/FUV, *J. Geophys. Res.*, *110*, A11302, doi:10.1029/2004JA010848.
Sakanoi, T., Y. Akiya, A. Yamazaki, Y. Otsuka, A. Saito, and I. Yoshikawa (2011), Imaging observation of the Earth's mesosphere, thermosphere and ionosphere by VISI of ISS-IMAP on the International Space Station, *IEEJ Trans. Fund. Mater.*, *131*(12), 983–988, doi:10.1541/ieejfms.131.983.
Salby, M. L., and P. F. Callaghan (2001), Seasonal amplification of the 2-day wave: Relationship between normal mode and instability, *J. Atmos. Sci.*, *58*, 1858–1869.
Salby, M. L., D. L. Hartmann, P. L. Bailey, and J. C. Gille (1984), Evidence for equatorial Kelvin modes in Nimbus-7 LIMS, *J. Atmos. Sci.*, *41*(2), 220–235, doi:10.1175/1520-0469(1984)041<0220:EFEKMI>2.0.CO;2.
Sassi, F., and H.-L. Liu (2014), Westward traveling planetary wave events in the lower thermosphere during solar minimum conditions simulated by SD-WACCM-X, *J. Atmos. Sol. Terr. Phys.*, *119*, 11–26, doi:10.1016/j.jastp.2014.06.009.
Sassi, F., D. Kinnison, B. A. Boville, R. R. Garcia, and R. G. Roble (2004), Effect of El Niño-Southern Oscillation on the dynamical, thermal, and chemical structure of the middle atmosphere, *J. Geophys. Res.*, *109*, D17108, doi:10.1029/2003JD004434.
Sassi, F., H.-L. Liu, J. Ma, and R. R. Garcia (2013), The lower thermosphere during the Northern Hemisphere winter of 2009: A modeling study using high-altitude data assimilation products in WACCM-X, *J. Geophys. Res. Atmos.*, *118*, 8954–8968, doi:10.1002/jgrd.50632.
Sassi, F., H.-L. Liu, and J. T. Emmert (2016), Traveling planetary-scale waves in the lower thermosphere: Effects on neutral density and composition during solar minimum conditions, *J. Geophys. Res. Space Physics*, *121*, 1780–1801, doi:10.1002/2015JA022082.
Sato, K., T. Kumakura, and M. Takahashi (1999), Gravity waves appearing in a high-resolution GCM simulation, *J. Atmos. Sci.*, *56*, 1005–1018, doi:10.1175/1520-0469(1999)056<1005:GWAIAH>2.0.CO;2.
Scaife, A. A., and I. N. James (2000), Response of the stratosphere to interannual variability of tropospheric planetary waves, *Q. J. R. Meteorol. Soc.*, *126*, 275–297.
Scherhag, R. (1952), Die explosionsartigen stratospärenerwärmungen des spätwinters 1951-1952, *Ber. Dtsch. Wetterdienst (US Zone)*, *6*, 51–63.
She, C.-Y., et al. (2004), Tidal perturbations and variability in mesopause region over Fort Collins, CO (41N, 105W): Continuous multi-day temperature and wind lidar observations, *Geophys. Res. Lett.*, *31*, L24111, doi:10.1029/2004GL021165.
Shen, B.-W. (2014), Nonlinear feedback in a five-dimensional Lorenz model, *J. Atmos. Sci.*, *71*, 1701–1723, doi:10.1175/JAS-D-13-0223.1.
Shiokawa, K., M. K. Ejiri, Y. Otsuka, T. Ogawa, M. Kubota, K. Igarashi, A. Saito, and T. Nakamura (2000), Multi-point observation of short-period mesospheric gravity waves over Japan during the FRONT campaign, *Geophys. Res. Lett.*, *27*, 4057–4060, doi:10.1029/2000GL011917.
Shiokawa, K., Y. Otsuka, and T. Ogawa (2009), Propagation characteristics of nighttime mesospheric and thermospheric waves observed by optical mesosphere thermosphere imagers at middle and low latitudes, *Earth Planets Space*, *61*, 479–491.

Siskind, D. E. (2014), Simulations of the winter stratopause and summer mesopause at varying spatial resolutions, *J. Geophys. Res. Atmos.*, *119*, 461–470, doi:10.1002/2013JD020985.
Siskind, D. E., F. Sassi, C. E. Randall, V. L. Harvey, M. E. Hervig, and S. M. Bailey (2015), Is a high-altitude meteorological analysis necessary to simulate thermosphere-stratosphere coupling?, *Geophys. Res. Lett.*, *42*, 8225–8230, doi:10.1002/2015GL065838.
Sridharan, S., T. Tsuda, T. Nakamura, and T. Horinouchi (2008), The 5–8-day Kelvin and Rossby waves in the tropics as revealed by ground and satellite-based observations, *J. Meteorol. Soc. Jpn. Ser. II*, *86*, 43–55, doi:10.2151/jmsj.86.43.
Sridharan, S., S. Sathishkumar, and S. Gurubaran (2012), Variabilities of mesospheric tides during sudden stratospheric warming events of 2006 and 2009 and their relationship with ozone and water vapour, *J. Atmos. Terr. Phys.*, *78*, 108–115, doi:10.1016/j.jastp.2011.03.013.
Talaat, E. R., J. H. Yee, and X. Zhu (2001), Observations of the 6.5-day wave in the mesosphere and lower thermosphere, *J. Geophys. Res.*, *106*, 20,715–20,723.
Talaat, E. R., J. H. Yee, and X. Zhu (2002), The 6.5-day wave in the tropical stratosphere and mesosphere, *J. Geophys. Res.*, *107*, 4133, doi:10.1029/2001JD000822.
Tsuda, T., M. Nishida, C. Rocken, and R. H. Ware (2000), A global morphology of gravity wave activity in the stratosphere revealed by the GPS occultation data (GPS/MET), *J. Geophys. Res.*, *105*, 7257–7273, doi:10.1029/1999JD901005.
Tsugawa, T., A. Saito, Y. Otsuka, M. Nishioka, T. Maruyama, H. Kato, T. Nagatsuma, and K. T. Murata (2011), Ionospheric disturbances detected by GPS total electron content observation after the 2011 off the Pacific coast of Tohoku Earthquake, *Earth Planets Space*, *63*, 875–879, doi:10.5047/eps.2011.06.035.
Tunbridge, V. M., D. J. Sandford, and N. J. Mitchell (2011), Zonal wave numbers of the summertime 2 day planetary wave observed in the mesosphere by EOS Aura Microwave Limb Sounder, *J. Geophys. Res.*, *116*, D11103, doi:10.1029/2010JD014567.
Vadas, S. L. (2007), Horizontal and vertical propagation and dissipation of gravity waves in the thermosphere from lower atmospheric and thermospheric sources, *J. Geophys. Res.*, *112*, 06405, doi:10.1029/2006JA011845.
Vadas, S. L., and D. C. Fritts (2001), Gravity wave radiation and mean responses to local body forces in the atmosphere, *J. Atmos. Sci.*, *58*, 2249–2279.
Vadas, S. L., and H.-L. Liu (2013), Numerical modeling of the large-scale neutral and plasma responses to the body forces created by the dissipation of gravity waves from 6 h of deep convection in Brazil, *J. Geophys. Res. Space Physics*, *118*, 2593–2617, doi:10.1002/jgra.50249.
Walterscheid, R. L. (1981), Inertio-gravity wave-induced accelerations of mean flow having an imposed periodic component: Implications for tidal observations in the meteor region, *J. Geophys. Res.*, *86*, 9698–9706.
Walterscheid, R. L., and M. P. Hickey (2005), Acoustic waves generated by gusty flow over hilly terrain, *J. Geophys. Res.*, *110*, A10307, doi:10.1029/2005JA011166.
Walterscheid, R. L., G. Schubert, and D. G. Brinkman (2003), Acoustic waves in the upper mesosphere and lower thermosphere generated by deep tropical convection, *J. Geophys. Res. Space Physics*, *108*, 1392, doi:10.1029/2003JA010065.
Wan, W., Z. Ren, F. Ding, J. Xiong, L. Liu, B. Ning, B. Zhao, G. Li, and M.-L. Zhang (2012), A simulation study for the couplings between DE3 tide and longitudinal WN4 structure in the thermosphere and ionosphere, *J. Atmos. Sol. Terr. Phys.*, *90-91*, 52–60, doi:10.1016/j.jastp.2012.04.011.
Wang, H., R. A. Akmaev, T.-W. Fang, T. J. Fuller-Rowell, F. Wu, N. Maruyama, and M. D. Iredell (2014), First forecast of a sudden stratospheric warming with a coupled whole-atmosphere/ionosphere model idea, *J. Geophys. Res. Space Physics*, *119*, 2079–2089, doi:10.1002/2013JA019481.
Wang, L., and M. A. Geller (2003), Morphology of gravity-wave energy as observed from 4 years (1998–2001) of high vertical resolution U.S. radiosonde data, *J. Geophys. Res.*, *108*, 4489, doi:10.1029/2002JD002786.
Warner, K., and J. Oberheide (2014), Nonmigrating tidal heating and MLT tidal wind variability due to the El Niño/Southern Oscillation, *J. Geophys. Res. Atmos.*, *119*(3), 1249–1265, doi:10.1002/2013JD020407.
Watanabe, S., and S. Miyahara (2009), Quantification of the gravity wave forcing of the migrating diurnal tide in a gravity wave-resolving general circulation model, *J. Geophys. Res.*, *114*, D07110, doi:10.1029/2008JD011218.
Watanabe, S., Y. Kawatani, Y. Tomikawa, K. Miyazaki, M. Takahashi, and K. Sato (2008), General aspects of a T213L256 middle atmosphere general circulation model, *J. Geophys. Res.*, *113*, D12110, doi:10.1029/2008JD010026.
Wright, C. J., N. P. Hindley, and N. J. Mitchell (2016), Combining AIRS and MLS observations for three-dimensional gravity wave measurement, *Geophys. Res. Lett.*, *43*, 884–893, doi:10.1002/2015GL067233.
Wu, D. L., and S. D. Eckermann (2008), Global gravity wave variances from Aura MLS: Characteristics and interpretation, *J. Atmos. Sci.*, *65*, 3695–3718.
Wu, D. L., P. B. Hays, W. R. Skinner, A. R. Marshall, M. D. Burrage, R. S. Lieberman, and D. A. Ortland (1993), Observations of the quasi 2-day wave from the high-resolution Doppler imager on UARS, *Geophys. Res. Lett.*, *20*, 2853–2856.
Wu, D. L., P. B. Hays, and W. R. Skinner (1994), Observations of the 5-day wave in the mesosphere and lower thermosphere, *Geophys. Res. Lett.*, *21*, 2733–2736.
Wu, Q., and S. Nozawa (2015), Mesospheric and thermospheric observations of the January 2010 stratospheric warming event, *J. Atmos. Sol. Terr. Phys.*, *123*, 22–38, doi:10.1016/j.jastp.2014.11.006.
Wu, Q., D. A. Ortland, S. C. Solomon, W. R. Skinner, and R. J. Niciejewski (2011), Global distribution, seasonal, and inter-annual variations of mesospheric semidiurnal tide observed by TIMED TIDI, *J. Atmos. Solar Terr. Phys.*, *73*, 2482–2502, doi:10.1016/j.jastp.2011.08.007.
Wu, Q., et al. (2008a), Global distribution and inter-annual variations of mesospheric and lower thermospheric neutral wind diurnal tide, part 1: Migrating tide, *J. Geophys. Res.*, *113*, A05308, doi:10.1029/2007JA012542.
Wu, Q., et al. (2008b), Global distribution and inter-annual variations of mesospheric and lower thermospheric neutral wind diurnal tide, part 2: Non-migrating tide, *J. Geophys. Res.*, *113*, A05309, doi:10.1029/2007JA012543.
Wu, T.-W., J. D. Huba, J. Krall, D. C. Fritts, and B. Laughman (2015), Seeding equatorial spread *F* with turbulent gravity waves: Phasing effects, *Geophys. Res. Lett.*, *42*, 15–21, doi:10.1002/2014GL062348.
Xu, J., A. K. Smith, H.-L. Liu, W. Yuan, Q. Wu, G. Jiang, M. G. Mlynczak, J. M. R. III, and S. J. Franke (2009), Seasonal and QBO variations in the migrating diurnal tide observed by TIMED, *J. Geophys. Res.*, *114*, D13107, doi:10.1029/2008JD011298.
Xu, J., et al. (2015), Concentric gravity waves over northern China observed by an airglow imager network and satellites, *J. Geophys. Res. Atmos.*, *120*, 11,058–11,078, doi:10.1002/2015JD023786.
Yamashita, C., H.-L. Liu, and X. Chu (2010), Gravity wave variations during the 2009 stratospheric sudden warming as revealed by ECMWF-T799 and observations, *Geophys. Res. Lett.*, *37*, L22806, doi:10.1029/2010GL045437.
Yamazaki, Y. (2013), Large lunar tidal effects in the equatorial electrojet during northern winter and its relation to stratospheric sudden warming events, *J. Geophys. Res. Space Physics*, *118*, 7268–7271, doi:10.1002/2013JA019215.
Yamazaki, Y., and A. D. Richmond (2013), A theory of ionospheric response to upward-propagating tides: Electrodynamic effects and tidal mixing effects, *J. Geophys. Res. Space Physics*, *118*, 5891–5905, doi:10.1002/jgra.50487.

Yamazaki, Y., A. D. Richmond, and K. Yumoto (2012), Stratospheric warmings and the geomagnetic lunar tide: 1958–2007, *J. Geophys. Res.*, *117*, A04301, doi:10.1029/2012JA017514.
Yamazaki, Y., A. D. Richmond, A. Maute, H.-L. Liu, N. Pedatella, and F. Sassi (2014), On the day-to-day variation of the equatorial electrojet during quiet periods, *J. Geophys. Res. Space Physics*, *119*, 6966–6980, doi:10.1002/2014JA020243.
Yiğit, E., A. D. Aylward, and A. S. Medvedev (2008), Parameterization of the effects of vertically propagating gravity waves for thermosphere general circulation models: Sensitivity study, *J. Geophys. Res.*, *113*, D19106, doi:10.1029/2008JD010135.
Yoden, S. (1987a), Bifurcation properties of a stratospheric vacillation, *J. Atmos. Sci.*, *44*, 1723–1733.
Yoden, S. (1987b), Dynamical aspects of stratospheric vacillations in a highly truncated model, *J. Atmos. Sci.*, *44*, 3683–3695.
Yue, J., and W. Wang (2014), Changes of thermospheric composition and ionospheric density caused by quasi 2-day wave dissipation, *J. Geophys. Res. Space Physics*, *119*, 2069–2078, doi:10.1002/2013JA019725.
Yue, J., H.-L. Liu, and L. C. Chang (2012a), Numerical investigation of the quasi 2 day wave in the mesosphere and lower thermosphere, *J. Geophys. Res.*, *117*, D05111, doi:10.1029/2011JD016574.
Yue, J., W. Wang, A. D. Richmond, and H.-L. Liu (2012b), Quasi-two-day wave coupling of the mesosphere and lower thermosphere-ionosphere in the TIME-GCM: Two-day oscillations in the ionosphere, *J. Geophys. Res.*, *117*, A07305, doi:10.1029/2012JA017815.
Yue, X., W. S. Schreiner, J. Lei, C. Rocken, D. C. Hunt, Y.-H. Kuo, and W. Wan (2010), Global ionospheric response observed by COSMIC satellites during the January 2009 stratospheric sudden warming event, *J. Geophys. Res.*, *115*, A00G09, doi:10.1029/2010JA015466.
Zettergren, M. D., and J. B. Snively (2013), Ionospheric signatures of acoustic waves generated by transient tropospheric forcing, *Geophys. Res. Lett.*, *40*, 5345–5349, doi:10.1002/2013GL058018.